HHS Public Access

Author manuscript

Nat Immunol. Author manuscript; available in PMC 2021 January 02.

Published in final edited form as:

Nat Immunol. 2020 July ; 21(7): 746–755. doi:10.1038/s41590-020-0695-4.

Interferon-mediated reprogramming of membrane cholesterol to evade bacterial toxins

Quan D. Zhou[1,2], **Xun Chi**[3], **Min Sub Lee**[1], **Wei Yuan Hsieh**[3], **Jonathan J. Mkrtchyan**[3], **An-Chieh Feng**[3], **Cuiwen He**[4], **Autumn G York**[1,7,8], **Viet L. Bui**[3], **Eliza B. Kronenberger**[3], **Alessandra Ferrari**[6], **Xu Xiao**[6], **Allison E. Daly**[3], **Elizabeth J. Tarling**[4], **Robert Damoiseaux**[1], **Philip O. Scumpia**[3,4], **Stephen T. Smale**[3], **Kevin J. Williams**[5], **Peter Tontonoz**[5,6], **Steven J. Bensinger**[1,3]

[1]Department of Molecular and Medical Pharmacology, University of California, Los Angeles, CA 90095

[2]Department of Surgical Oncology, The First Affiliated Hospital, School of Medicine, Zhejiang University, Hangzhou, Zhejiang 310003, P.R. China

[3]Department of Microbiology, Immunology and Molecular Genetics, University of California, Los Angeles, CA 90095

[4]Department of Medicine, David Geffen School of Medicine, University of California, Los Angeles CA 90095

[5]Department of Biological Chemistry, University of California, Los Angeles, CA 90095

[6]Department of Pathology and Laboratory Medicine, University of California, Los Angeles, CA 90095

[7]Department of Immunobiology, Yale University School of Medicine, New Haven, CT 06520, USA

[8]Howard Hughes Medical Institute, Yale University, New Haven, CT 06520, USA

Abstract

Plasma membranes of animal cells are enriched for cholesterol. Cholesterol-dependent cytolysins (CDCs) are pore forming toxins secreted by bacteria that target membrane cholesterol for their effector function. Phagocytes are essential for clearance of CDC-producing bacteria; however, mechanisms these cells use to evade the deleterious effects of CDCs are largely unknown. Here, we report that interferon (IFN) signals convey resistance to CDC-induced pores on macrophages

Correspondence: Steven J. Bensinger (sbensinger@mednet.ucla.edu).

Author contributions S.J.B. conceived the study. Q.D.Z. led all experimental design and execution of experiments. X.C. co-designed and performed all flow cytometry-based experiments and data analysis. V.L.B., W.Y.H., and J.J.M. contributed to flow cytometry experiments. J.J.M. and M.S.L. contributed to protein purification and staining experiments. Q.D.Z., M.S.L., and R.D. developed and performed live-cell imaging assays. C.H. performed NanoSIM analysis and contributed to protein purification. J.J.M. and E.B.K. contributed to RNA analysis. W.Y.H. and A.G.Y. performed GC-MS analysis with help from Q.D.Z. and E.B.K. K.J.W conducted lipidomics studies. X.X., A.F., P.T. and E.J.T. contributed to *Abcg1*, *Abca1*, and SCAP KO studies. A.E.D. analyzed gene expression data. A.-C.F., P.O.S. M.S.L. and S.T.S conceptualized and developed the *in vivo* SLO challenge assay. W.Y.H. contributed to data visualization. S.J.B., Q.D.Z, W.Y.H., X.C. and P.T. contributed to construction of the manuscript.

Competing Interests: None.

and neutrophils. We traced IFN-mediated resistance to CDCs to the rapid modulation of a specific pool of cholesterol in the plasma membrane of macrophages, without changing total cholesterol levels. Resistance to CDC pore formation requires production of the oxysterol 25-hydroxycholesterol, inhibition of cholesterol synthesis, and redistribution of cholesterol to an esterified cholesterol pool. Accordingly, blocking IFN's ability to reprogram cholesterol metabolism abrogates cellular protection and renders mice more susceptible to CDC-induced tissue damage. These studies illuminate targeted regulation of membrane cholesterol content as a host-defense strategy.

Introduction

Cholesterol is the most abundant lipid in the plasma membrane and an important determinant of its biochemical and biophysical properties[1, 2, 3, 4]. Cellular cholesterol homeostasis is maintained through a combination of synthesis, import, storage and efflux pathways. While each pathway may be engaged independently, they are often co-regulated to ensure that sufficient cholesterol is available for a cell and to avoid deleterious accumulation. Recent studies indicate that sterol metabolism pathways of immune cells, in particular macrophages, can be rapidly reprogrammed to support their effector functions[5, 6, 7, 8]. Toll-like receptors and interferons have been shown to mediate reprogramming of cholesterol homeostasis by rapidly decreasing cholesterol synthetic flux [9, 10], increasing cholesterol ester storage in lipid droplets[11, 12], and stimulating the production of cholesterol derivatives such as the oxysterol 25-hydroxycholesterol (25HC) [5, 13, 14]. This reprogramming of sterol homeostasis facilitates host defense responses through a variety of mechanisms including blockade of viral entry, regulation of innate immune receptor signaling, immune cell skewing, and increasing macrophage phagocytic capacity. Thus, coordinated regulation of sterol metabolic pathways in immune cells is now viewed as a fundamental component of the host defense response.

Given the essential requirement for cholesterol in animal membranes, it is not surprising that microorganisms and viruses have evolved strategies that take advantage of cholesterol availability in membranes to facilitate pathogenesis [15, 16, 17, 18]. Cholesterol-dependent cytolysins (CDCs) are a group of secreted toxins produced mainly by Gram-positive bacteria that depend on membrane cholesterol for their pathogenic function[19, 20, 21]. CDC binding to cholesterol in the plasma membrane facilitates CDC oligomerization and pore formation, resulting in loss of membrane integrity, reduced efficacy of anti-microbial function, and cell death [22, 23]. Cells have repair mechanisms by which they minimize the deleterious effects of CDC toxins. Damaged plasma membranes can be internalized and resealed[24, 25] or may bleb and be subsequently shed as microvesicles[26]. However, it appears that phagocytes attempting membrane repair may become hypo-responsive to pro-inflammatory stimuli through shedding of toll-like receptors (TLRs) and cytokine receptors[23]. Thus, host membrane repair mechanisms, which preserve phagocyte survival, also reduce their effectiveness for anti-microbial host defense. As to whether phagocytes or other immune cells have evolved specific strategies that facilitate evasion from these pore-forming toxins remains less well understood.

Here we report that activation of pattern recognition receptors (PRR) signaling on macrophages influences susceptibility to CDC-induced loss of membrane integrity and function. We show that interferon (IFN) signals convey resistance to CDC-mediated membrane damage on phagocytes by reprogramming their cellular cholesterol metabolism, whereas Myd88-dependent TLR signals do not induce protection. Mechanistic studies revealed that IFNs mediate resistance to CDCs by decreasing their binding to the plasma membrane. The decrease in CDC binding required coordinated inhibition of new cholesterol synthesis and an increase in the esterification of a small amount of pre-existing cellular cholesterol. IFN-mediated changes in cholesterol homeostasis were also dependent on the endogenous production of 25HC, and we found that loss of the enzyme cholesterol 25-hydroxylase (CH25H) resulted in increased binding of CDC proteins at the plasma membrane. Accordingly, perturbations in sterol metabolic pathways abrogated IFNs protective effects for phagocytes and renders mice more susceptible to CDC-induced tissue damage. Together these findings indicate that IFN-mediated changes to sterol metabolism convey resistance to CDCs by decreasing a small pool of cholesterol in the plasma membrane, and suggest that specifically targeting this pool of cholesterol could facilitate host defense to CDC-producing pathogenic bacteria.

Results

Interferons mediate resistance to cholesterol-dependent cytolysins

It has been shown that activation of macrophages through Toll-like receptor (TLR) and cytokine signals reprograms their lipid metabolism [5, 6, 7, 8, 10, 27], leading us to ask if these changes in lipid metabolism altered sensitivity to CDCs. To address this question, mouse bone marrow-derived macrophages (BMDMs) were stimulated with TLR1/2, TLR3, TLR4, TLR7 or TLR9 agonists for 24 h and then challenged with the CDC perfringolysin O (PFO) for up to 60 min. The membrane impermeable dye propidium iodide (PI) was added to the media just before PFO treatment to assess pore formation and loss of membrane integrity in macrophages, but not cell death. As expected, PFO increased the percentage of PI^+ cells over time in unstimulated macrophages (Fig. 1a and Extended Data Fig. 1a). Activation of macrophages with TLR1/2, TLR4, TLR7 or TLR9 agonists resulted in little or no change in sensitivity to PFO treatment (Fig. 1a and Extended Data Fig. 1a, b). In contrast, TLR3-mediated activation markedly decreased macrophages sensitivity to PFO challenge (Fig. 1a and Extended Data Fig. 1a).

It was unexpected that TLR3 activation, which is associated with anti-viral responses, provided a substantial measure of protection to PFO-induced pore formation. Since a primary inflammatory outcome of TLR3 signaling is the generation of type I IFNs[28, 29], we tested whether type I IFN stimulation alone would also convey resistance to PFO. We observed that treatment of macrophages with IFN-β overnight also conveyed resistance to PFO (Fig. 1b and Extended Data Fig. 1c). IFN-γ treatment of macrophage cultures also induced resistance to PFO challenge (Fig. 1b and Extended Data Fig. 1c), indicating that protection is mediated by both type I and type II IFNs. We also tested whether activation of other pattern recognition receptors (PRRs) that generate type I IFN responses[30] would also protect macrophages from CDC challenge. The stimulator of interferon genes (STING;

TMEM173) is activated by cyclic di-nucleotides generated by intracellular microbes (e.g., *Listeria monocytogenes*)[31]. We found that treatment of BMDM cultures with STING ligands (cGAMP or c-di-GMP) for 24 h also resulted in protection from PFO challenge (Fig. 1c and Extended Data Fig. 1d). The nucleotide-binding oligomerization domain-containing protein 2 (NOD2)—an intracellular receptor stimulated by peptidoglycans produced by Gram-positive microbes— has also been shown to induce low levels of type I IFN during bacterial infections[32]. Consistent with this, activation of NOD2 with N-Glycolyl-MDP resulted in modest protection to PFO challenge (Fig. 1c and Extended Data Fig. 1d). Importantly, we observed a similar pattern of IFN-mediated resistance for macrophages challenged with the CDCs streptolysin-O (SLO) or anthrolysin-O (ALO) (Fig. 1d, e and Extended Data Fig. 1e–g), indicating that the protection conveyed by IFNs may be a general strategy for resistance to the larger group of pore-forming CDCs.

We were surprised that TLR1/2 activation did not induce resistance to CDCs given the important role of this TLR signaling module in mediating immune responses to Gram-positive bacteria. However, we found that macrophages co-stimulated with TLR1/2 agonist and IFN-β acquired some measure of resistance to PFO and SLO (Fig. 1f, g and Extended Data Fig. 1h, i), indicating that IFN signals can induce a “resistant” phenotype regardless of PRR engaged. We also found that IFN stimulation (4 h) of purified mouse bone marrow neutrophils resulted in resistance to CDC-mediated loss of membrane integrity (Fig. 1h), demonstrating that IFN’s ability to induce protection can be observed in other phagocytic innate immune cells. Importantly, IFN stimulation (IFN-γ or IFN-β) largely preserved the ability of macrophages to phagocytose extracellular bacteria (i.e. *Staphylococcus aureus*) when challenged with PFO (Fig. 1i). Together, these data demonstrate that autocrine or paracrine IFN signals induce resistance to CDC-mediated pore formation, resulting in preservation of macrophage membrane integrity and phagocytic function.

Interferons decrease binding of CDCs to the plasma membrane

To understand if the observed changes in CDC sensitivity could be due to altered CDC binding to the plasma membrane, we performed studies on IFN-stimulated macrophages with fluorescently labeled anthrolysin O domain 4 (ALO-D4), a modified CDC toxin with markedly reduced pore-forming capacity, but retains near normal binding characteristics to plasma membrane[33, 34, 35, 36]. We found that the binding of ALO-D4 to IFN-β− or IFN-γ −stimulated macrophages was significantly decreased when compared to control macrophages (Fig. 2a). High-throughput imaging analysis of macrophage cultures (greater than 3000 macrophages/condition) stimulated with IFN-β, IFN-γ, STING ligand, or TLR3 ligand showed a marked reduction in the average intensity of ALO-D4 binding (Fig. 2b, c, d, e). By contrast, ALO-D4 binding was maintained or modestly increased in TLR1/2-stimulated macrophages (Fig. 2f, g), consistent with our data indicating the TLR1/2 stimulated macrophages maintained sensitivity to CDC-induced loss of membrane integrity. A similar decrease in ALO-D4 binding in response to either IFN-α or IFN-β was observed in human peripheral blood-derived macrophages (hPBMCs) (Fig. 2h, i). Likewise, 6 h stimulation of purified mouse bone marrow neutrophils with IFNs also decreased ALO-D4 binding (Extended Data Fig. 2a, b). Time course studies showed that a decrease in ALO-D4 binding could be observed within 2 h of IFN stimulation of BMDMs (Fig. 2j, k). As

expected, the decrease in ALO-D4 signal induced by IFN-β (or PRRs which induce type I IFNs) was abrogated in type I IFN receptor–deficient macrophages (IFNAR-deficient) (Extended Data Fig. 2c, d). However, overnight IFN-γ treatment of IFNAR-deficient macrophages decreased ALO-D4 binding (Fig. 2l, m), demonstrating that resistance induced by type I and type II IFN cytokines are not dependent on each other. In combination, these data indicate that the protection from CDCs is induced quickly in response to IFNs, and suggest that protection is mediated by reduced binding of CDCs to the plasma membrane.

Interferons decrease a small pool of membrane cholesterol targeted by CDCs

Next, we asked whether IFN signals altered the binding of CDCs to the plasma membrane by decreasing macrophage cholesterol content. To address this, we performed gas chromatography-mass spectrometry (GC-MS) to quantify total cellular cholesterol amounts on IFN–stimulated BMDMs. We observed that IFNs modestly increased the total amount of cholesterol in macrophages (Fig. 3a). Likewise, we observed that STING or TLR3 activation, which induce robust type I IFN responses, also increased total cholesterol content (Extended Data Fig. 3a). Thus, the protection mediated by IFNs could not be attributed to a global decrease in cholesterol content. We also performed GC-MS on purified plasma membrane from quiescent and IFN-γ stimulated macrophages; however, no difference in cholesterol pool size was observed (Fig. 3b and Extended Data Fig. 3b). We also stained BMDMs with Fillipin III, a bacterial product that binds to unesterified cholesterol in membranes and forms a fluorescent complex[37]. Consistent with our mass spectrometry studies, no change in Fillipin III staining was observed in response to IFN-stimulation (Extended Data Fig. 3c). We also investigated whether IFN stimulation disrupted sphingomyelin-associated cholesterol in the plasma membrane. Ostreolysin A (OlyA) is a protein that specifically binds to cholesterol when associated with sphingomyelin[38]. To assess whether IFNs altered this pool of cholesterol in the plasma membrane of macrophages we applied nanoscale secondary ion mass spectrometry (NanoSIMS)[39, 40] using stable isotope-labeled ALO-D4 and OlyA proteins. Consistent with the fluorescent ALO-D4 imaging studies, we observed a decrease in ^{15}N-labeled ALO-D4 binding in response to IFN-β stimulation (Fig. 3c). In contrast, ^{15}N-OlyA binding remained unchanged (Fig. 3c). High-throughput imaging studies with fluorescent-labeled OlyA showed a similar binding pattern for unstimulated and IFN-treated macrophage cultures (Extended Data Fig. 3d, e). Cholera toxin B (CTB) staining also showed no change, indicating that IFN signaling does not disrupt GM1 ganglioside-containing microdomains of the plasma membrane (Extended Data Fig. 3f). Together, these data support the conclusion that substantial amounts of cholesterol remain in the plasma membrane in association with sphingolipids after IFN stimulation[38]. Consistent with this concept, briefly treating IFN-stimulated macrophages with sphingomyelinase (SMase)[39] restored ALO-D4 binding (Fig. 3d, e). Thus, we conclude that CDCs are targeting a small fraction of non-sphingomyelin-associated cholesterol within the plasma membrane, and that IFN signaling alters the availability of this pool of cholesterol to reduce CDC binding to phagocytes.

Cholesterol synthesis is linked to CDC susceptibility

We and others have previously reported that IFN signaling can reduce *de novo* cholesterol synthesis in macrophages[7, 9, 10]. Thus, we considered the possibility that the changes in

CDC sensitivity was linked to cholesterol biosynthetic capacity of activated macrophages. To address this, we performed [^{13}C]-glucose tracer enrichment studies on PRR- and IFN-stimulated macrophages. IFN-β and IFN-γ stimulation markedly decreased macrophage cholesterol synthesis (Fig. 4a). Likewise, activation of STING or TLR3 also decreased cholesterol biosynthesis (Extended data Fig. 4a, b). In contrast, TLR1/2- TLR7- and TLR9-activation increased the amounts of synthesized cholesterol accumulated (Extended Data Fig. 4b). These data largely mirror the differential sensitivity to CDCs that we observed in PRR- and IFN-stimulated macrophages, leading us to hypothesize that cholesterol biosynthetic flux determines susceptibility to CDC-induced plasma membrane damage. Consistent with this, pharmacologic inhibition of cholesterol synthesis using simvastatin reduced ALO-D4 binding to otherwise unstimulated macrophages and protected from CDC-mediated membrane damage (Fig. 4b, c and Extended Data Fig. 4c). We also asked if genetic attenuation of cholesterol synthesis would intrinsically convey resistance to CDC recognition. Loss of the SREBP chaperone protein SCAP has been shown to attenuated cholesterol synthesis in macrophages[10]. We observed that quiescent SCAP-deficient macrophages exhibited decreased ALO-D4 binding, and accordingly, these cells were protected from PFO challenge (Fig. 4d, e). The oxysterol 25-hydroxycholesterol (25HC) is an endogenous inhibitor of cholesterol biosynthesis through its ability to induce degradation of 3-Hydroxy-3-Methylglutaryl-CoA Reductase (HMGCR)—the rate limiting enzyme in cholesterol synthesis—and inhibition of the SREBP transcriptional axis[41, 42]. Thus, we asked if treating macrophage cultures with this oxysterol would also alter ALO-D4 binding. To that end, wild-type quiescent macrophages were treated with 25HC (3 μM) for 4 h. We found that treatment with 25HC markedly reduced ALO-D4 binding (Fig. 4f, g). Together, these data support the concept that the pool of newly synthesized cholesterol, rather than the total cholesterol available in the plasma membrane, is linked to the sensitivity or resistance of macrophages to CDC-mediated toxicity.

Production of 25-hydroxycholesterol is required for resistance to CDCs

IFNs have a well-defined role in inducing the conversion of cholesterol into 25HC via the enzyme CH25H in macrophages[5, 13, 14]. Thus, we next asked if the endogenous production of 25HC is required for IFN-mediated protection to CDCs. To address this, control and CH25H-deficient macrophages were stimulated with IFNs and ALO-D4 binding was assessed. We observed that neither IFN-β or IFN-γ treatment of macrophage cultures reduced ALO-D4 binding (Fig. 5a, b). Correspondingly, we found that stimulating CH25H-deficient macrophages with IFN-β or IFN-γ was unable to induce protection to either PFO or SLO challenge (Fig 5c, d and Extended Data Fig. 5a, b). We also observed that, in contrast to control macrophages, IFN-treatment of CH25H-deficient macrophages were unable to maintain efficient phagocytosis of bacteria when challenged with PFO (Fig. 5e). Importantly, provisioning of 25HC to cultures of CH25H KO or control macrophages protected them from CDC-induced pore formation (Fig. 5f), and largely restored their ability to phagocytose bacteria (Fig. 5e). Thus, endogenous production of 25HC appears to be critical for macrophage protection to CDCs.

Next, we sought to better define the mechanism by which IFN signaling and the production of 25HC mediate protection to CDCs. Our studies to this point had correlated a decrease in

cholesterol biosynthesis with protection to CDC challenge, leading us to ask if loss of CH25H altered IFN-mediated reduction in the cholesterol synthesis. [^{13}C]-glucose tracer enrichment studies showed that loss of CH25H resulted in basally higher production of cholesterol compared to control macrophages, but did not alter total cholesterol content (Fig. 5g). IFN-β stimulation was able to reduce cholesterol synthesis in both control and CH25H-deficient macrophages, but the reduction was attenuated in the absence of CH25H, resulting a synthetic profile that more closely resembled that observed in unstimulated control macrophages (Fig. 5g). Treating CH25H-deficient macrophages with simvastatin was sufficient to reduce ALO-D4 binding, supporting the concept that 25HC's ability to regulate cholesterol synthetic flux is an important mechanism by which IFNs mediate protection from CDCs (Fig. 5h, i).

Cholesterol esterification contributes to CDC resistance of macrophages

We observed that IFNs induce a number of genes involved in cholesterol esterification and efflux (Fig. 6a), leading us to ask if these processes were also necessary for IFN-mediated protection from CDCs. As expected, IFN-treatment of macrophages increased cholesterol ester formation[43, 44] (Fig. 6b). Unexpectedly, we found that cholesterol in culture media was not required for accumulation of esterified cholesterol in response to IFNs (Extended Data Fig. 6a), indicating that the source of cholesterol for esterification can be derived from host cell membranes rather than from the extracellular milieu. Pharmacologic inhibition of the cholesterol esterification enzymes acyl-CoA:cholesterol acyltransferase (ACAT1 and 2) partially attenuated the protection from PFO-mediated pore formation conveyed by IFN signaling (Fig. 6c and Extended Data Fig. 6b). 25HC has also been shown to mediate cholesterol ester (CE) formation[45, 46], thus we asked if CH25H-deficiency influenced cholesterol ester production in response to IFN signals. We found that quiescent CH25H-deficient macrophages had modestly increased levels of cholesterol esters and were able to increase this pool to control levels in response to IFN stimulation (Extended Data Fig. 6c). Consistent with this, we observed that treatment of CH25H-deficient macrophages with an ACAT inhibitor further increased ALO-D4 binding and increased their susceptibility to CDC-mediated membrane damage (Fig. 6d and Extended Data Fig. 6d). These data indicate that synthesis of cholesterol esters in macrophages is required, in part, for resistance to CDCs.

To test whether cholesterol efflux was required for IFN-mediated protection to CDCs, we activated macrophages deficient in the key cholesterol efflux transporters ATP Binding Cassette Subfamily A Member 1 (ABCA1) or ATP Binding Cassette Subfamily G Member 1 (ABCG1) with IFN[11, 12]. We found that 24 h IFN treatment reduced ALO-D4 binding to both ABCA1- and ABCG1-deficient macrophages to a level similar to that of control macrophages (Extended Data Fig. 6e). No difference in susceptibility to CDC-mediated pore formation was observed between quiescent control and ABCA1-deficient macrophages (Fig. 6e). Furthermore IFN-treatment conveyed resistance to PFO challenge for ABCA1-deficient macrophages, indicating that efflux was unlikely to be an important component of the IFN-mediated protection under these conditions. However, we did find that pharmacologically enforcing cholesterol efflux by treating with LXR agonist GW3965 [47]for 24 h decreased ALO-D4 binding and provided robust protection against CDC in wild-type macrophages

(Fig. 6f, g). We also observed that LXR activation with GW3965 decreased ALO-D4 binding and conveyed protection for CH25H-deficient macrophages from PFO challenge (Fig. 6f, g), indicating that 25HC mediates protection by regulating synthesis of cholesterol rather than blocking CDCs at the membrane or inducing esterification. Taken together, these data support a model where IFNs reduce cholesterol synthesis and increase esterification of free cholesterol to reduce the pool size of the cholesterol in the plasma membrane targeted by CDCs.

25HC mediates protection to CDC induced tissue damage

Finally, we asked if reprogramming of cholesterol homeostasis would influence CDC susceptibility *in vivo*. To that end, SLO was injected into the skin of control and CH25H-deficient mice. Injection sites were visually monitored for up to 48 h for the appearance of erythema and ulceration. Injection of SLO into the skin of control mice resulted in modest erythema within 24 h and small ulcers 48 h after injection (Fig. 7a, and Extended Data Fig. 7a; lesions indicated with white arrow). In contrast, CH25H-deficient mice developed severe erythema within 24 h which progressed to ulcerative lesions that were up to 6-fold larger in area than those of their WT counterparts (Fig. 7a and Extended Data Fig. 7a). Histologic examination of the tissues confirmed greater epidermal ulceration area, along with a greater depth of tissue necrosis into the deep dermis and in some cases the adipose tissue in CH25H-deficient mice (Fig. 7b). We also asked if injecting 25HC into the dermis would protect mice from CDC-induced tissue damage. For these studies, we used ALO challenge since we find that ALO reliably induces larger skin lesions in control mice than SLO. We found that pre-injection of 25HC into the dermis of mice for 6 h markedly reduced ALO-induced tissue damage (Fig. 7c and Extended Data Fig. 7b). Histologic examination revealed that in most cases 25HC pretreatment completely prevented tissue damage, or in cases with damage, 25HC pretreatment reduced both ulcer area and depth (Fig. 7d). Thus, we conclude that generation of 25HC and the consequent ability to reprogram cholesterol metabolism protects mice from CDC-mediated tissue damage.

Discussion

Immune cells presumably have evolved strategies to evade the deleterious effects of virulence factors in order to efficiently combat pathogens and protect the host from damage. In this study, we delineate a mechanism by which IFN signals alter the abundance of a small pool of cholesterol in the plasma membrane in order to protect macrophages and neutrophils from pathogen-produced toxins. We think it likely that IFN-mediated reprogramming of cholesterol homeostasis will extend into other cell types, such as endothelium, adipocytes and epithelium, given the extent of the tissue damage observed in the skin of CH25H KO mice in response to CDC challenge. Mechanistically, we find that inhibition of new cholesterol synthesis through the actions of CH25H is required to induce this protection mechanism. We also find that the IFN-mediated conversion of cholesterol into cholesterol esters is required for maximal protection. In combination, IFN regulation of these distinct, but interrelated cholesterol metabolic pathways ensure that the cholesterol pool targeted by CDCs remains small, and consequently macrophages and neutrophils retain their function. These data also imply that pharmacologic manipulation of the cholesterol homeostatic

machinery in the skin might decrease tissue damage associated with deleterious effects of Gram-positive infections observed in necrotizing fasciitis or similar soft tissue infections. However, it will be necessary to determine if manipulating cholesterol homeostasis in infected tissues interferes with other host defense pathways and clearance of microbes.

One unexpected finding of our studies is that the IFN-induced changes in plasma membrane cholesterol are restricted to a very small fraction of the total membrane cholesterol. The exact pool of cholesterol in the plasma membrane targeted by CDCs remains poorly characterized[19, 20] and our data suggest that a very minor fraction of cholesterol in the plasma membrane is required for CDC binding and pore formation. Cholesterol is not evenly distributed across the plasma membrane[2, 48]. The majority of cholesterol in the plasma membrane is tightly associated sphingomyelins or other phospholipids in microdomains[38, 49]. Recent elegant studies provide evidence for distinct pools of cholesterol within the plasma membrane. These studies describe a small pool of cholesterol—termed “accessible” cholesterol—that is in rapid equilibrium with the ER cholesterol pool and consequently the cholesterol biosynthetic machinery[48]. We suspect that this is the pool of cholesterol that is targeted by CDCs and rapidly reduced upon IFN signaling. Our data indicate that this IFN-dependent reduction of the “accessible” cholesterol pool occurs through the combined actions of the ACAT enzymes and inhibition of cholesterol biosynthesis. We cannot rule out the possibility that IFN signals also move cholesterol from “accessible” pool laterally or vertically into other domains in the plasma membrane. It will be of considerable interest to determine the spatial distribution of the “accessible” cholesterol pool within the plasma membrane, and how this specific cholesterol pool relates to canonical domains that have been described to exist in the plasma membrane.

We also believe that there will be other cholesterol metabolic pathways involved in this protective mechanism. We find that IFNs induce changes in ALO-D4 binding within 2 h, thus it seems likely that direct signaling events downstream of the IFN receptors initiate this process and it will be of interest to define the cholesterol transport machinery involved in this rapid removal of this small pool of cholesterol from the plasma membrane. The observation that both type I and II IFNs regulate a broad cassette of genes involved in cellular cholesterol homeostasis (e.g., efflux, esterification, synthesis, intracellular trafficking) leads us to surmise that there is considerable pressure to sequester or limit accessible or free cholesterol from pathogens, and it will be of interest to determine the pathophysiologic context where this reshaping of membrane cholesterol homeostasis contributes to host defense. These observations also imply that other mechanisms that can influence the pool size of accessible cholesterol, such as metabolic dysfunction could influence the susceptibility of cells to these pore-forming toxins. Consistent with this notion, it has been shown that diabetes and obesity are independent risk factors for necrotizing fasciitis[50, 51] and we posit that restoring cellular cholesterol homeostasis with drugs that target cholesterol metabolic machinery might serve to decrease the severity of disease in these patients. In support of this idea, we find that enforced cholesterol efflux through the activation of LXR can induce protection independent of IFN signaling. Likewise, injecting 25HC into the skin protected the dermis from ALO-induced damage, providing initial proof of concept that metabolic manipulation could be an adjunctive approach to conventional antimicrobials.

In conclusion, these studies provide evidence that rapid remodeling of the lipid content of membranes is employed as a host defense strategy by macrophages and neutrophils. Given the breadth of microbial and viral proteins that target host lipids, we propose that signal-specific reprogramming of the lipidome of cells will be a fundamentally important strategy for host cells to evade different pathogens.

Methods

Mouse strains.—WT and gene-targeted mice were purchased from The Jackson Laboratory if possible: WT C57BL/6J (JAX 000664). B6;129S6-*Ch25h*^{tm1Rus}/J (*Ch25h*$^{-/-}$, JAX 016263), B6(Cg)-*Ifnar1*$^{tm1.2Ees}$/J (*Ifnar*$^{-/-}$, JAX 028288). SCAP-deficient macrophages were generated from *LysM*-Cre × *Scap*$^{fl/fl}$ as previously described[10]. ABCA1- and ABCG1-deficient macrophages were generated from *LysM*-Cre × *Abca1*$^{fl/fl}$ or *LysM*-Cre × *Abcg1*$^{fl/fl}$ animals as previously described[50, 51]. All mice used for BMDM were male with age between 8–16 weeks. For i*n vivo* CDC injections, mice were female with age between 8–12 weeks. All mice were maintained in pathogen free facilities of the University of California, Los Angeles. All experiments on mice and tissues collected from mice were performed in strict accordance with University of California, Los Angeles policy on the humane and ethical treatment of animals.

Peripheral blood mononuclear cells (PBMCs) derived macrophages.—Human monocyte-derived monocytes were isolated from leukopacks using standard Ficoll isolation procedures and plastic adherence. Isolation of monocytes was conducted by the UCLA CFAR Virology Core. Monocytes were differentiated into macrophage with 50 ng/mL human GM-CSF (Peprotech, 300–03) in IMDM (Hyclone) media with 10% FBS and 1% v/v pen/strep for 7 days prior to experimental use.

Mouse cells.—Bone marrow cells were differentiated into macrophages in DMEM containing 10% v/v FBS (HyClone, GE SH3007103), 5% v/v M-CSF conditioned media, 1% v/v pen/strep, 1% v/v glutamine (Invitrogen) 0.5% v/v sodium pyruvate (Invitrogen) for 7–9 days prior to experimental use. Cells were changed to media with 5% FBS at the time of stimulation. Mouse neutrophils were isolated from the bone marrow using EasySep™ Mouse Neutrophil Enrichment Kit (19762) from StemCell following manufacturer's protocol.

Reagents.—PRR ligands: LPS (Invivogen, tlrl-smlps), Poly(I:C) (Invivogen, tlrl-pic (HMW)), Pam3CSK4 (Invivogen, tlrl-pms), CL307 (Invivogen, tlrl-c307), ODN1668 (invivogen, tlrl-1668), 2′,3′-cGAMP (Invivogen tlrl-nacga23), c-di-GMP (Invivogen, tlrl-cdg), 5′ppp-dsRNA (Invivogen, tlrl-3prn), iE-DAP (Invivogen, tlrl-dap), N-Glycolyl-MDP (Invivogen, tlrl-gmdp). Cytokines: recombinant Murine IFN-γ (Peprotech, 315–05), recombinant Mouse IFN-β1 (carrier-free, BioLegend, 581302), recombinant human IFN-β (Peprotech, 300–02BC), IFN-α is a kind gift from R. Modlin lab (UCLA). Hyclone IMDM media (16750–088) and FBS (SH3007103) were purchased from VWR. PFO is a kind gift from A.S. Divakaruni lab [52] (Agilent, 102504–100). Streptolysin O from *Streptococcus pyogenes* (gamma irradiated, Sigma S0149–25KU), 58–035 (Sigma. S9318), and

Simvastatin (Sigma, S6196–5MG) were purchased from Sigma-Aldrich. LXR agonist GW3965 was purchased from Sigma-Aldrich (G6295–5MG).

Cholesterol Ester Analysis.—Macrophages were cultured in 6-well dishes (Fisher, 08–772-1B) and stimulated with TLR ligands as described above. 48 h post-stimulation, cells were imaged for cell count as previously described[10], scraped and spun down in PBS, and snap-frozen as cell pellets. A modified Bligh and Dyer extraction[53] was carried out on samples. Prior to biphasic extraction, a 13-lipid class Lipidyzer Internal Standard Mix is added to each sample (AB Sciex, 5040156). Following two successive extractions, pooled organic layers were dried down in a Genevac EZ-2 Elite. Lipid samples were resuspended in 1:1 methanol/dichloromethane with 10 mM Ammonium Acetate and transferred to robovials (ThermoFisher, 10800107) for analysis. Samples were analyzed on the Sciex Lipidyzer Platform for targeted quantitative measurement of 1100 lipid species across 13 classes. Differential Mobility Device on Lipidyzer was tuned with SelexION tuning kit (Sciex, 5040141). Instrument settings, tuning settings, and MRM list available upon request. Data analysis performed on Lipidyzer software. Quantitative values were normalized to cell counts.

Isotope Enrichment Experiments.—Day 8 differentiated BMDMs were transferred to complete media containing 50% [^{13}C]-glucose (Cambridge Isotope Laboratories, CLM-1396-MPT-PK) with or without TLR stimulation for 48 h before collection. Analysis of labeled fatty acids and cholesterol was performed as described previously[10, 54, 55]. The relative contributions of synthesis to the total cholesterol pool over the 48 h-labeling period were determined by fitting the isotopologue distributions for cholesterol in a model similar to Isotopomer Spectral Analysis (ISA) as described previously [10, 54, 55].

Gene expression analysis.—RNA was extracted from all cells with Trizol (ThermoFisher, 15596–018) using manufacturer's protocols. cDNA was synthesized with high-capacity cDNA reverse transcription kit (Applied Biosystems, 4368814) as per manufacturer's instructions (700 ng/μL RNA per cDNA synthesis reaction). Quantitative PCR (qPCR) was conducted on the Roche LightCycler 480 using SYBR Green Master Mix (Kapa Biosciences) or PowerUp™ SYBR™ Green Master Mix (ThermoFisher, A25778) and 0.5 μmol/L primers. Relative expression values are normalized to control gene (*Rplp0*) and expressed in terms of linear relative mRNA values.

CDC Permeabilization Live Imaging.—BMDMs and neutrophils were seeded 5×10^4/well on 96-well plates (E&K Scientific, EK-25090, Greiner). Cells were left for 2 days before stimulation. Cells were pretreated with TLR ligands for 2–24 h depending on the experiment. For live-cell imaging, culture media were replaced by 37 °C PBS with 0.05% BSA, 1 μg/mL propidium iodide (PI) (VWR, 80057–368) and 5 μg/mL Hoechst 33342 (ThermoFisher, H3570). Then cells were challenged by spiking recombinant PFO (final concentration 1 nM), gamma-irradiated SLO (final concentration 22 nM), or recombinant ALO (final concentration 1.5 nM), and plates were imaged every 10 min on Molecular Devices ImageXpress XL using a 20x Objective (Nikon Plan Fluor, 0.3 NA). SLO was activated with the addition of 10 mM DTT at 22 °C for 10 min. Total (Hoechst 33342-

positive) and permeabilized (PI-positive) cell number were assessed using MetaXpress Software with Powercore using the Multi-wavelength cell scoring module.

Macrophage phagocytosis assay.—BMDMs were seeded 1.5×10^5/well on 24-well plates. Cells were left for 1–3 days before stimulation. Cells were pretreated with TLR ligands for 24 h. PFO were diluted in PBS to a final concentration of 2 nM, and cells were left to incubate for 15 min at 37 °C, then cells were washed with PBS twice, and replaced with fresh BMDM media with 5% FBS. pHrodo™ Red *S. aureus* Bioparticles™ Conjugate (0.4 mg/mL) (ThermoFisher, A10010) were added on top of the macrophages and incubated for 1 h at 37 °C. To remove the un-phagocytosed apoptotic thymocytes or pHrodo™ Red Bioparticles™ Conjugate, cells were washed once with PBS and then subject to flow cytometry analysis.

Flow cytometry analysis.—BMDMs were lifted off the plates by scraping with the plunger of a 1 mL syringe and transferred to a 96-well round-bottom plate. After pelleting, cells were first incubated with TruStain FcX™ (anti-mouse CD16/32) Antibody (BioLegend, 101319, 1:500) in FACS buffer (PBS with 2% FBS, 1 mM EDTA) for 10 min on ice. Cells were then stained with antibodies for surface markers CD11b (BioLegend, 101207, 1:400) for 20 min on ice. After one wash with FACS buffer, cells were resuspended in FACS buffer with 1 μg/mL DAPI (ThermoFisher, D1306) and analyzed with Attune NxT Flow Cytometer. Data were analyzed by FlowJo V10.

Plasma membrane purification.—BMDMs were seeded at 8×10^6/plate on 10 cm tissue culture treated dishes. Cells were left for 2 days before stimulation. Cells were then treated with IFNs for 24 h. Plasma membrane purification were carried out by cell surface biotinylation followed by streptavidin affinity chromatography as previously described[36, 46].

Filipin III staining.—BMDMs were seeded at 1.5×10^5/well on 24-well plates. Cells were left for 1–3 days before stimulation. Cells were pretreated with TLR ligands for 24 h. Filipin III was purchased from Sigma-Aldrich (F4767) and resuspended in ethanol to 2 mg/mL. BMDMs were washed once with PBS and fixed with 3% paraformaldehyde for 15 min at 22 °C. Cells were then washed twice and stained with 100 μg/mL filipin III for 30 min at 22 °C covered in dark. After staining, cells were washed once with PBS and visualized by Zeiss Axio Observer. Z1.

Cholera Toxin B (CTB) Staining.—BMDMs were seeded at 1.5×10^5/well on 24-well plates and left for 1–3 days before stimulation. Cells were pretreated with IFNs for 24 h. BMDMs were lifted off the plates by scraping with the plunger of a 1 mL syringe and transferred to a 96-well round-bottom plate. CTB was purchased from ThermoFisher Scientific (C34777). Cells were stained with 1 μg/mL CTB for 10 min on ice. Cells were then resuspended in FACS buffer and analyzed with Attune NxT Flow Cytometer. Data were analyzed by FlowJo V10.

Preparation of [^{15}N] or [^{13}C] His-Tagged ALO-D4.—A plasmid for ALO-D4 (ALO amino acids 404–512 with C472A and S404C substitutions) was originally obtained from A. Radhakrishnan [36, 38] (University of Texas Southwestern Medical Center, Dallas), and [^{15}N]-

labeled ALO-D4 was prepared as described before[56]. Briefly, ALO-D4 was expressed in BL21 (DE3) pLysS *Escherichia coli* (Invitrogen) and induced with 1 mM isopropyl β-d-1-thiogalactopyranoside (IPTG) in 1 L of minimal medium containing 20.2 mM NH_4Cl and 2 g of glucose at 18 °C for 16 h. [^{15}N] NH_4Cl or [^{13}C]-glucose were used for [^{15}N] or [^{13}C]-ALO-D4, respectively. Cells were pelleted and lysed by sonication, and the lysate was centrifuged at 4 °C. The supernatant was mixed with 4 mL of HisPur Cobalt resin (50% bed volume; ThermoFisher Scientific). The mixture was loaded into a column and allowed to flow through by gravity. The column was washed, and [^{15}N] ALO-D4 was eluted with a buffer containing 300 mM imidazole. The eluates were pooled and concentrated to 1 mL with an Amicon 10 kDa cut off concentrator (Millipore). The purified [^{15}N] ALO-D4 was stored at 4 °C.

Preparation of His-Tagged ostreolysin A(OlyA) and Full-length ALO.—Plasmids for OlyA (with C62S C94S S151C substitution) and ALO were kind gifts from A. Radhakrishnan [38] (University of Texas Southwestern Medical Center, Dallas).

Preparation of Fluorescent ALO-D4, OlyA.—Purified protein was conjugated as described previously with slight modifications[10]. Briefly, cysteine-substituted ALO-D4 or OlyA were incubated with Alexa-488 or Alexa-594 (Life Technologies) at 4 °C overnight in 50 mM Tris-HCl (pH 7.5) and 150 mM NaCl (1x TBS) containing 1 mM Tris(2-carboxyethyl)phosphine hydrochloride (TCEP). Free dye was separated by extensive buffer exchange with 1x TBS in Amicon 10 kDa cut off concentrator (Millipore), and stored at 4 °C.

Binding of ALO-D4, OlyA to Cells.—Cells were seeded 1.5×10^5/well on PDL-coated coverslips (Neuvitro, fisher NC0672873) on a 24-well plate. After stimulation, cells were incubated with ALO-D4, or OlyA as described before[40]. Briefly, macrophages were washed three times for 10 min in PBS/Ca/Mg containing 0.2% (wt/vol) BSA. Cells were then incubated with ALO-D4, OlyA (all 20 μg/mL) in PBS/Ca/Mg containing 0.2% (wt/vol) BSA for 2 h at 4 °C. Unbound proteins were removed by washing with PBS/Ca^{2+}/Mg^{2+} three times for 2 min each.

Confocal Microscopy Analysis.—After fluorescently labeled ALO-D4, or OlyA binding, cells were fixed with 3% paraformaldehyde for 15 min and stained with 5 μg/mL DAPI, then washed twice with PBS/ Ca^{2+}/Mg^{2+} for imaging. Images were taken with an Axiovert 200M microscope and processed with Zen 2010 software (Zeiss). High-resolution images were taken by Zeiss LSM880.

Quantification of Fluorescence Intensity.—For signal quantification, cells were plated on 24-well plates (Cellvis, P24–0-N), treated, stained as above, and fixed cells in DPBS/Ca^{2+}/Mg^{2+} were imaged within 24 h. Images were taken at UCLA Molecular Screening Shared Resource core facility on a Molecular Device ImageXpress Confocal using a 20x Objective (Nikon Plan Fluor, 0.3 NA) on a Molecular Devices ImageXpress XL. Maximum projected cellular fluorescence intensity was assessed by MetaXpress Software with Powercore using the Multi-wavelength cell scoring module. Integrated fluorescent intensity profile were exported and analyzed by R with ggplot2 package or Graphpad Prism

8. Filipin III staining was quantified with FIJI by measuring fluorescent signals on plasma membranes.

NanoSIMS Sample Preparation.—As described before[56], after ALO-D4 or OlyA binding, cells were fixed with 4% paraformaldehyde (Electron Microscopy Sciences) and 2.5% glutaraldehyde (Electron Microscopy Sciences) in 0.1 M phosphate buffer (1.14 g NaH_2PO_4, 1.69 g Na_2HPO_4 in a 100 mL final volume of ddH_2O, pH 7.4) for 20 min at 4 °C followed by 1 h at 22 °C. The samples were washed three times for 7 min each in 0.1 M phosphate buffer, post-fixed with 1% osmium tetroxide (Electron Microscopy Sciences) in 0.1 M phosphate buffer for 45 min, and washed three times for 7 min each in ice-cold ddH_2O. Then cells were air-dried.

NanoSIMS Analyses.—As described before[40, 56], platinum-coated (5-nm) cells were analyzed with a nanoSIMS 50L instrument (CAMECA) with some modifications. Briefly, samples were bombarded with a focused $^{133}Cs+$ primary beam, and secondary ions (e.g., $^{12}C-$, $^{13}C-$, $^{16}O-$, $^{12}C^{14}N-$, $^{12}C^{15}N-$) and secondary electrons were collected. Before imaging, a high $^{133}Cs+$ primary beam (1-nA beam current; primary aperture D1 = 1) was used to presputter an area of 50 × 50 μm for 25 s to remove the platinum coating and implant $1^{33}Cs+$. In the same region, low-magnification images (~40 × 40 μm) were obtained with an ~2.5-pA beam current (primary aperture D1 = 2), a dwell time of 2.5 ms per pixel, and scans of 512 × 512 pixels. High-magnification images (~10 × 10 μm) were obtained with an ~0.8-pA beam current (primary aperture D1 = 3), a dwell time of ~10 ms per pixel, and scans of 512 × 512 pixels.

NanoSIMS Quantification.—To quantify $^{13}C/^{12}C$ and $^{15}N/^{14}N$ ratios in cells, we identified particles by SEM and/or $^{12}C-$, $^{12}C^{14}N-$, $^{16}O-$, or secondary electron nanoSIMS images, and regions of interest in the middle of the particles were defined with the OpenMIMS plugin in ImageJ (NIH). For each image, the mean $^{15}N/^{14}N$ and $^{13}C/^{12}C$ ratios of the regions of interest were measured by ImageJ and processed by Prism 7.0.

***In vivo* CDC injection.—**For SLO challenge studies, litter-matched control and *Ch25h*$^{-/-}$ C57BL/6J mice were shaved on the lower back and recovered overnight. On the next day, mice were intradermally injected with either PBS or SLO (8 kU/mouse). SLO was activated with 10 mM DTT at 22 °C. 48 h later, photographs of the skin lesions were taken, and the lesion area (in cm^2) was measured using the ImageJ software, followed by an unequal *t*-test. For ALO challenge studies, wild-type C57BL/6 mice were shaved on the lower back and were pre-injected intradermally with 25-hydroxycholesterol (10 mg/kg) or ethanol vehicle control for 6 h, followed by ALO injection (20 nM). Lesion sizes were quantified as above 48 h after ALO injection. Photographs of the skin lesions were taken at 48 h post ALO challenge, and lesion area (in cm^2) measured using the ImageJ software, followed by an unequal *t*-test. Tissue samples were collected for histological analysis in UCLA Translational and Pathology Core Laboratory.

Statistical analysis.—Experiments were conducted as three biological distinct independent replicates, unless otherwise stated. Statistical significance was determined using the GraphPad Prism software. For bar graphs, line graphs and scatter plot, data are shown as

the mean and the error bars depict the s.e.m. unless otherwise stated. For all CDC-permeabilization assays, an average of 800 cells were imaged per well and used for calculations. Statistical analysis for CDC-permeabilization curves were assessed from the time when first images taken after CDCs were added to cultures until the end of the assay at 60 minutes. Statistical tests used for each graph were specified in the legend.

Further Detailed information on experimental design and reagents can be found in the “Life Sciences Reporting Summary”.

Extended Data

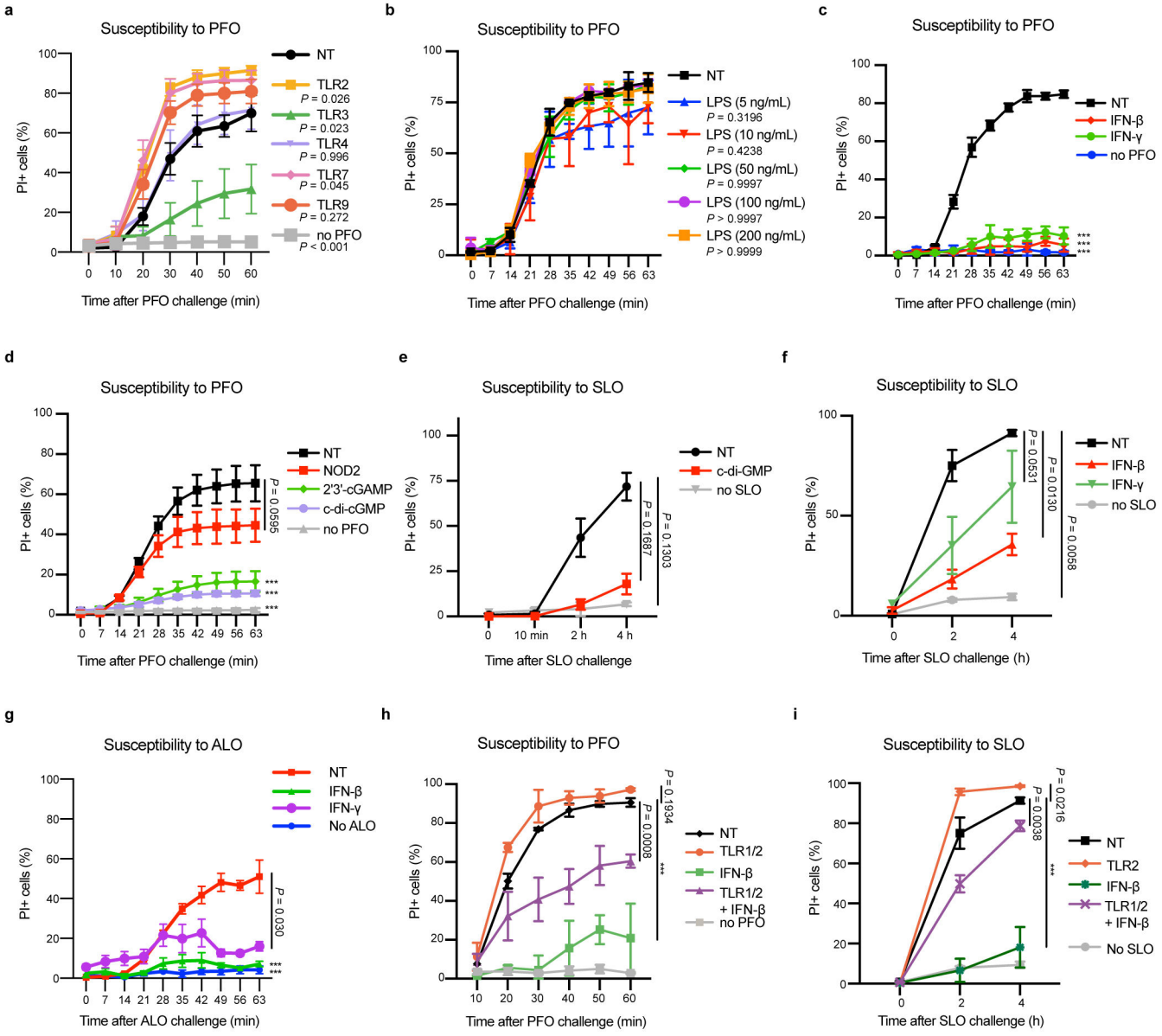

Extended Data Fig. 1.

Interferon signaling mediates resistance to cholesterol-dependent cytolysins. a, Percentage of PI-positive BMDMs treated with TLR1/2 agonist (Pam3CSK4; 50 ng/mL), TLR3 agonist (Poly(I:C); 1 μg/mL), TLR4 agonist (LPS; 50 ng/mL), TLR7 agonist (CL307; 100 nM), TLR9 (ODN1668; 100 nM) agonist, or unstimulated (NT) for 24 h and then challenged with PFO for up to 60 min in the presence of PI. Cells were imaged every 10 min to assess changes in PI incorporation. b, Percentage of PI-positive BMDMs treated with the various concentrations of TLR4 agonist for 24 h and then challenged with PFO for up to 60 min in the presence of PI. Cells were imaged every 7 min to assess changes in PI incorporation. c, Percentage of PI-positive BMDMs treated with IFN-β or IFN-γ (20 ng/mL) for 24 h and then challenged with PFO for 60 min in the presence of PI. d, Percentage of PI-positive BMDMs treated with NOD2 agonist (N-Glycolyl-MDP; 20 μg/ml), STING agonist (2’,3’cGAMP and c-di-GMP; both 2 μg/mL) for 24 h and then challenged with PFO for 60 min in the presence of PI. e, Percentage of PI-positive BMDMs treated with STING ligand for 24 h and then challenged with Streptolysin O (SLO) for 4 h in the presence of PI. f, Percentage of PI-positive BMDMs treated with IFN-β or IFN-γ (20 ng/mL) for 24 h and then challenged with SLO for 4 h in the presence of PI. g, Percentage of PI-positive BMDMs treated with IFN-β or IFN-γ (20 ng/mL) for 24 h and then challenged with ALO for 60 min in the presence of PI. h, Percentage of PI-positive BMDMs treated with IFN-β (100 ng/mL) or TLR1/2 agonist, or IFN-β (100 ng/mL) together with TLR1/2 agonist for 24 h and then challenged with PFO for 60 min in the presence of PI. i, Percentage of PI-positive BMDMs treated with IFN-β (100 ng/mL) or TLR1/2 agonist, or IFN-β (100 ng/mL) together with TLR1/2 agonist for 24 h and then challenged with SLO for 4 h in the presence of PI. Data are representatives of three independent experiments, and are shown as mean ± s.e.m. (n = 3). Statistical significance was determined using an RM one-way ANOVA with Dunnett’s correction (a-g) or a two-way ANOVA with Dunnett’s correction (h, i). ***P<0.001.

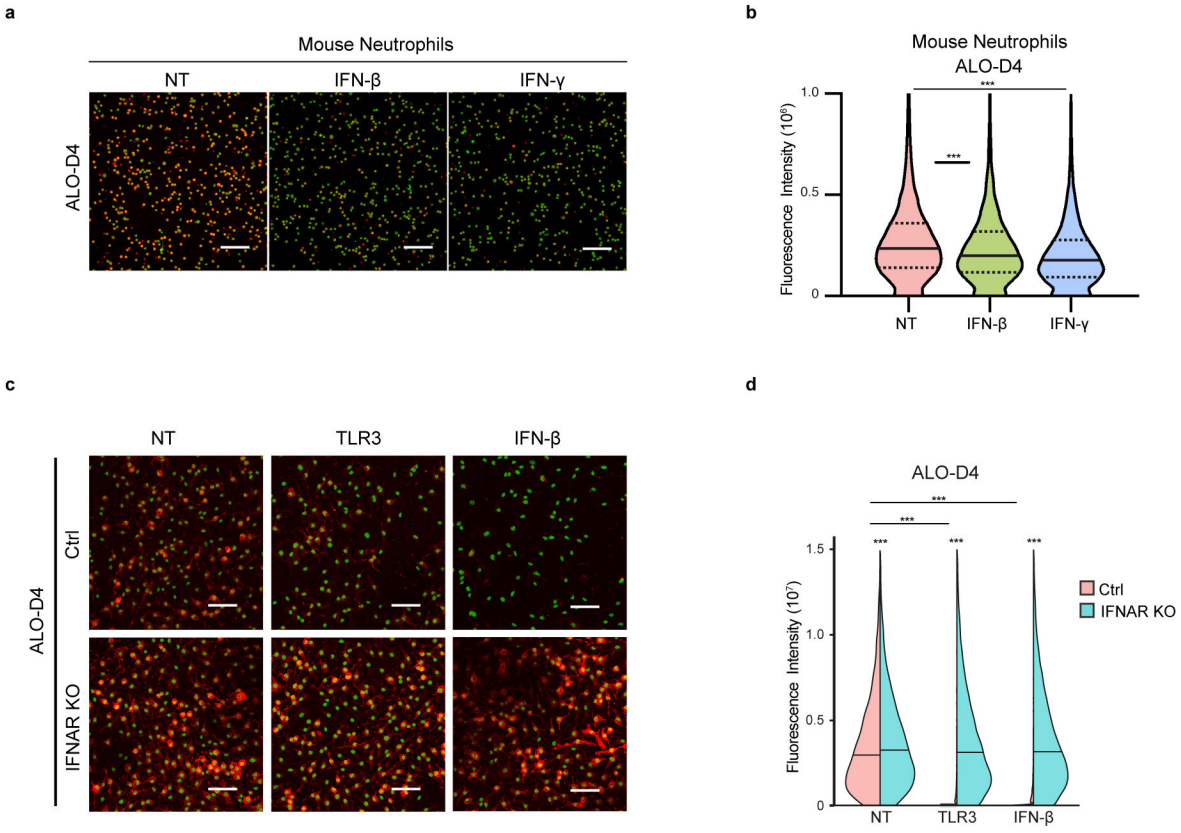

Extended Data Fig. 2.

IFN signals decrease plasma membrane binding to ALO-D4 protein. a, Confocal images of neutrophils stimulated with IFN-β or IFN-γ (20 ng/mL) for 6 h, and then stained with fluorescent ALO-D4 and DAPI. b, Violin plots of cellular fluorescent intensity quantified from a (n = 20334, 18546, 16290). c, Confocal images of WT or type I interferon receptor–deficient (IFNAR KO) BMDMs stimulated with TLR3 agonist (1 μg/mL) or IFN-β (20 ng/mL) for 24 h, and then stained with fluorescent ALO-D4 and DAPI. d, Violin plots of cellular fluorescent intensity quantified from c (n = 5543, 6682, 4673, 8231, 5201, 7906). Data are representatives of three independent experiments. Violin plots are shown with median (solid lines in b, d) and 25% and 75% percentiles (dashed lines in b), and statistical significance was determined using a Kruskal-Wallis test with Dunn's correction. ***P<0.001. Scale bars in a, c represent 50 μm.

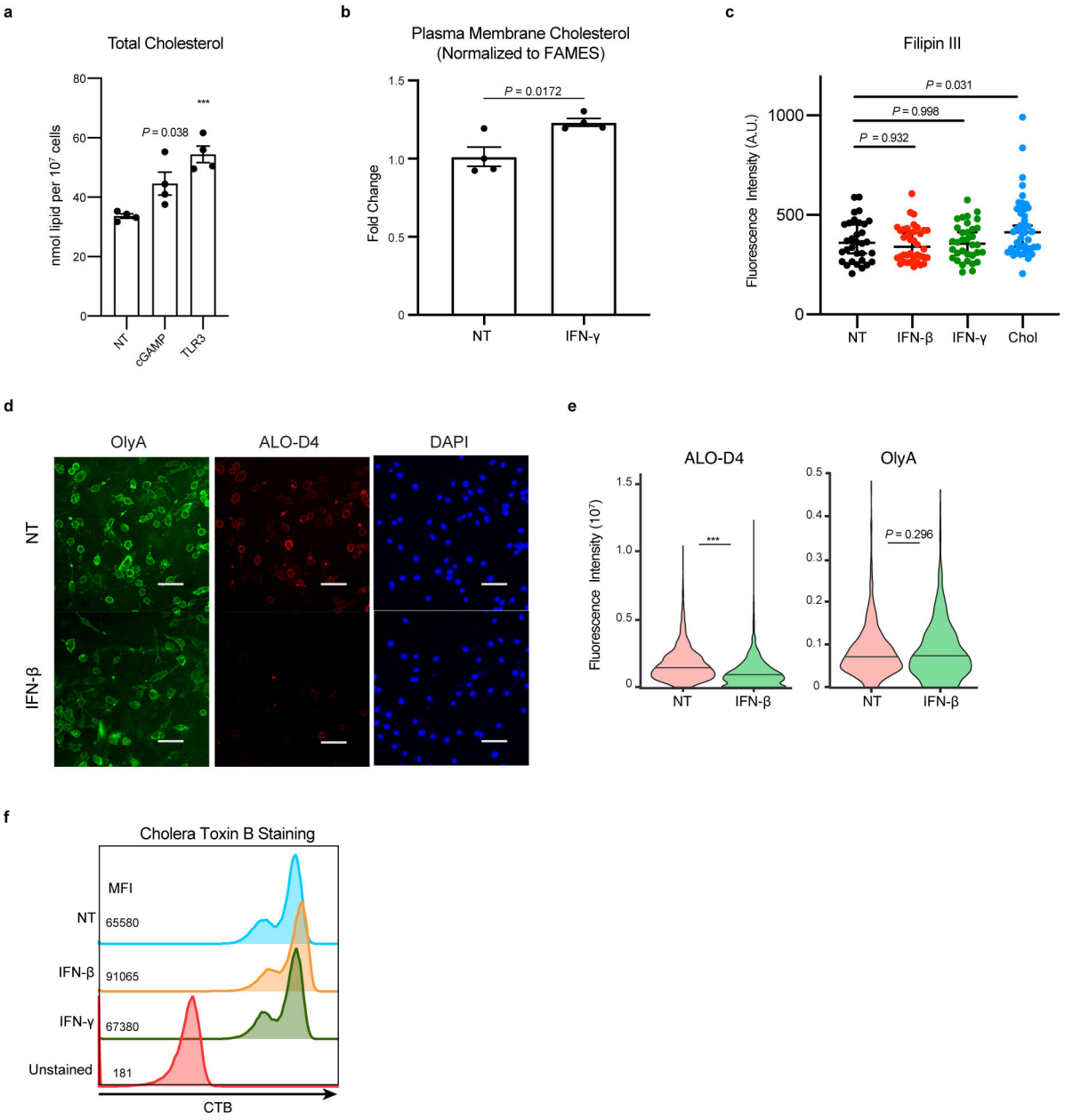

Extended Data Fig. 3.

IFN signals reprogram cholesterol metabolism to decrease the pool of cholesterol targeted by CDCs. a, Total cholesterol (nmol/107 cells) from C57BL/6 bone marrow–derived macrophages (BMDMs) stimulated with cGAMP (2 μg/mL), TLR3 agonist (Poly(I:C); 1 μg/mL), or unstimulated (NT) for 48 h. Total cholesterol was determined by GC-MS (n = 4). b, Total plasma membrane cholesterol (normalized to total FAMEs) from C57BL/6 bone marrow–derived macrophages (BMDMs) stimulated with IFN-γ (40 ng/mL) or unstimulated (NT) for 24 h (n = 4). c, Relative Fillipin III fluorescence intensity of plasma membranes of untreated macrophages or macrophages stimulated with IFN-β (20 ng/mL) or IFN-γ (20 ng/mL) for 24 h (n = 32, 38, 34, 42). MβCD-Cholesterol loaded macrophages indicate dynamic range of Fillipin III fluorescence and are included as a positive control. d, Confocal

images of BMDM stimulated with IFN-β (20 ng/mL) for 24 h, and then stained with fluorescent ALO-D4 or OlyA and DAPI. Scale bar, 50 μm. e, Violin plots of cellular fluorescent intensity quantified from d (n = 2225, 2021, 2225, 2021). f, Cholera Toxin B staining of BMDM stimulated with IFN-β or IFN-γ (20 ng/mL) for 24 h. Median fluorescence intensity (MFI) are indicated on the left. Data are representative of three (a, d, e, f) independent experiments, three independent samples (c) or from 4 biological replicates (b). Data in a-c are shown as mean ± s.e.m., violin plots in e are shown with median (solid lines). Statistical significance was determined using an unpaired two-tailed Student's t-test (a, b), a one-way ANOVA with Dunnett's correction (c), or a two-tailed Mann–Whitney test (e) ***P<0.001.

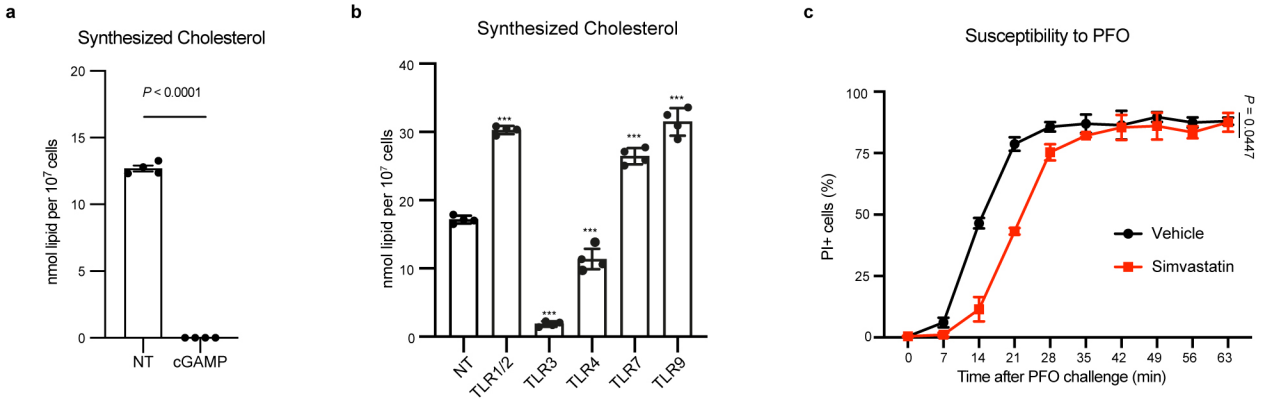

Extended Data Fig. 4.

Cholesterol synthesis is linked to CDC susceptibility. a, Net synthesized cholesterol (nmol/107 cells) from C57BL/6 bone marrow–derived macrophages (BMDMs) stimulated with cGAMP (2 μg/mL), or unstimulated (NT) for 48 h. Synthesized cholesterol was determined by GC-MS and isotopomer spectral analysis modeling (n = 4). b, Net synthesized cholesterol (nmol/107 cells) from C57BL/6 bone marrow–derived macrophages (BMDMs) stimulated with TLR1/2 agonist (Pam3CSK4; 50 ng/mL), TLR3 agonist (Poly(I:C); 1 μg/mL), TLR4 agonist (LPS; 50 ng/mL), TLR7 agonist (CL307; 100 nM), TLR9 (ODN1668; 100 nM) agonist, or unstimulated (NT) for 48 h. Synthesized cholesterol was determined by GC-MS and isotopomer spectral analysis modeling (n = 4). c, Percentage of PI–positive WT BMDMs treated with Simvastatin (1 μM) for 4 h and then challenged with PFO for 60 min in the presence of PI (n = 3). Data are representative of three independent experiments and are shown as mean + s.e.m. Statistical significance was determined using an unpaired two-tailed Student's t-test (a), a one-way ANOVA with Dunnett's correction (b), or a paired two-tailed Student's t-test (c). ***P<0.001.

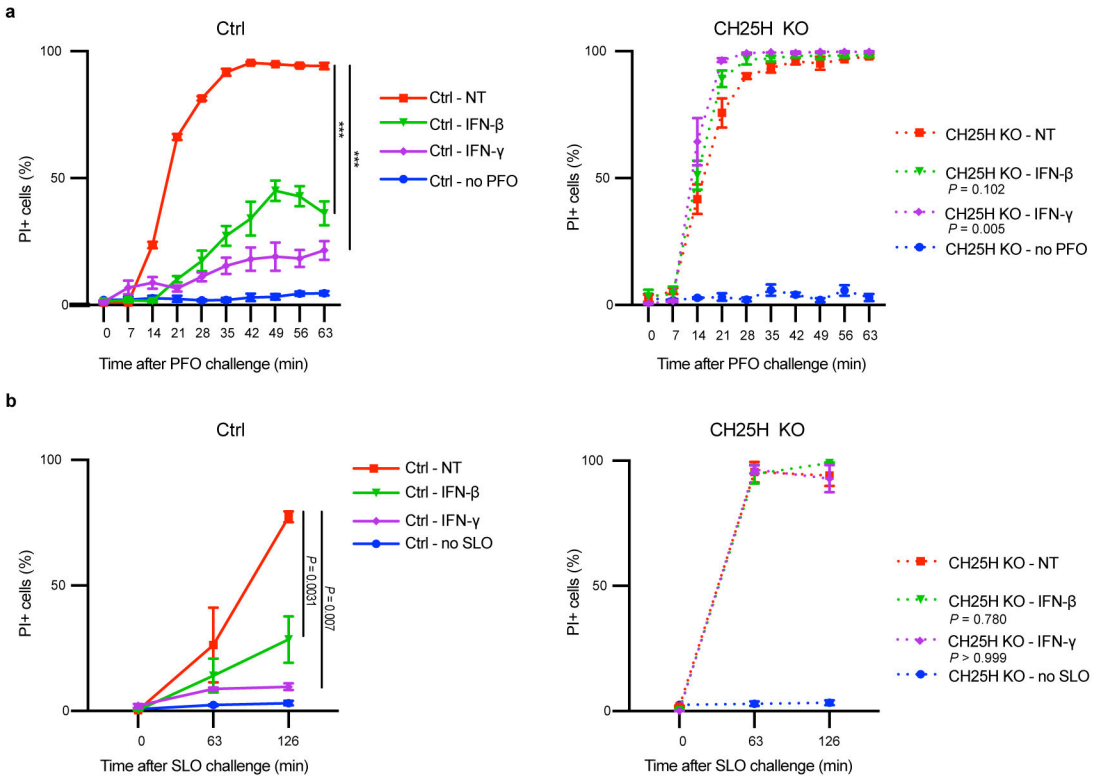

Extended Data Fig. 5.

Production of 25-hydroxycholesterol is required to maintain changes in plasma membrane cholesterol and mediates resistance to CDCs. a, Percentage of PI–positive control or CH25H KO BMDMs stimulated with IFNs (20 ng/mL) for 24 h and then challenged with PFO for 60 minutes in the presence of PI. b, Percentage of PI–positive control or CH25H KO BMDMs stimulated with IFNs (20 ng/mL) for 24 h and then challenged with SLO for 2 h in the presence of PI. Data are representative of three independent experiments and are shown as mean + s.e.m. (n = 3) and statistical significance was determined using a two-way ANOVA with Dunnett's correction. ***P<0.001.

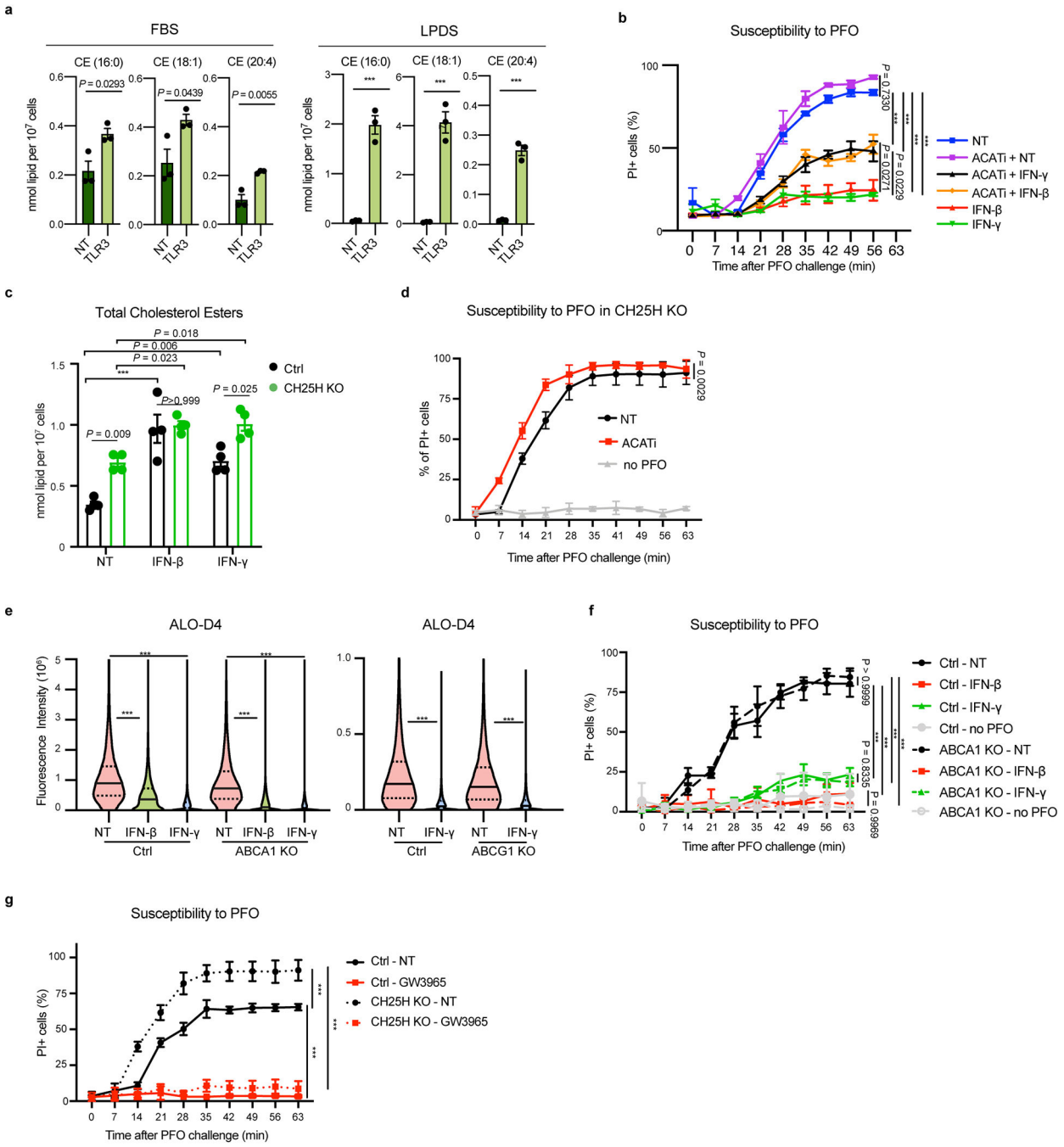

Extended Data Fig. 6.

Cholesterol esterification contributes to CDC resistance of macrophages. a, Quantification (nmol/107 cells) of cholesterol ester species (16:0. 18:1, 20:4) in BMDMs stimulated with TLR3 agonist (1 μg/mL) in FBS or LPDS for 48 h. CE species pool sizes were determined by direct infusion MS. b, Percentage of PI–positive WT BMDMs treated with IFN-β, or IFN-γ (20 ng/mL), or in combination with ACATi 58–035 (4.3 μM) for 24 h and then challenged with PFO for 60 min in the presence of PI. c, Quantification (nmol/107 cells) of total cholesterol ester (CE) in control or CH25H KO BMDMs stimulated with IFN-β (20

ng/mL) or IFN-γ (20 ng/mL) for 48 h. CE pool sizes were determined by direct infusion mass spectrometry. d, Percentage of PI-positive CH25H KO BMDMs treated with ACATi 58–035 (4.3 μM) for 24 h and then challenged PFO for 60 min in the presence of PI. e, Violin plots of cellular fluorescent intensity quantified from control or ABCA1 KO or ABCG1 KO BMDMs stimulated with IFNs (20 ng/mL) for 24 h and then stained with fluorescent ALO-D4 and DAPI (n = 5943, 4126, 5727, 6914, 5740, 7898; n=7201, 7532, 7563, 7417). f, Percentage of PI-positive control or ABCA1 KO BMDMs treated with IFNs (20 ng/mL) for 24 h and then challenged PFO for 60 min in the presence of PI. g, Percentage of PI-positive control or CH25H KO BMDMs treated with LXR agonist GW3965 (1 μM) for 24 h and then challenged PFO for 60 min in the presence of PI. Data are representatives of two (a, c) or three (b, d, e, f, g) independent experiments. Data in a, b, c, d, f and g are shown as mean + s.e.m. (n = 3 in a, b, d, g; n = 4 in c). Violin plots in e are shown with median (solid lines) and 25% and 75% percentiles (dashed lines). Statistical significance was determined using an unpaired two-tailed Student's t-test (a), a two-way ANOVA with Tukey's correction (b, c, f, g), a paired two-tailed Student's t-test (d), or a Kruskal–Wallis test with Dunn's correction (e). ***P<0.001.

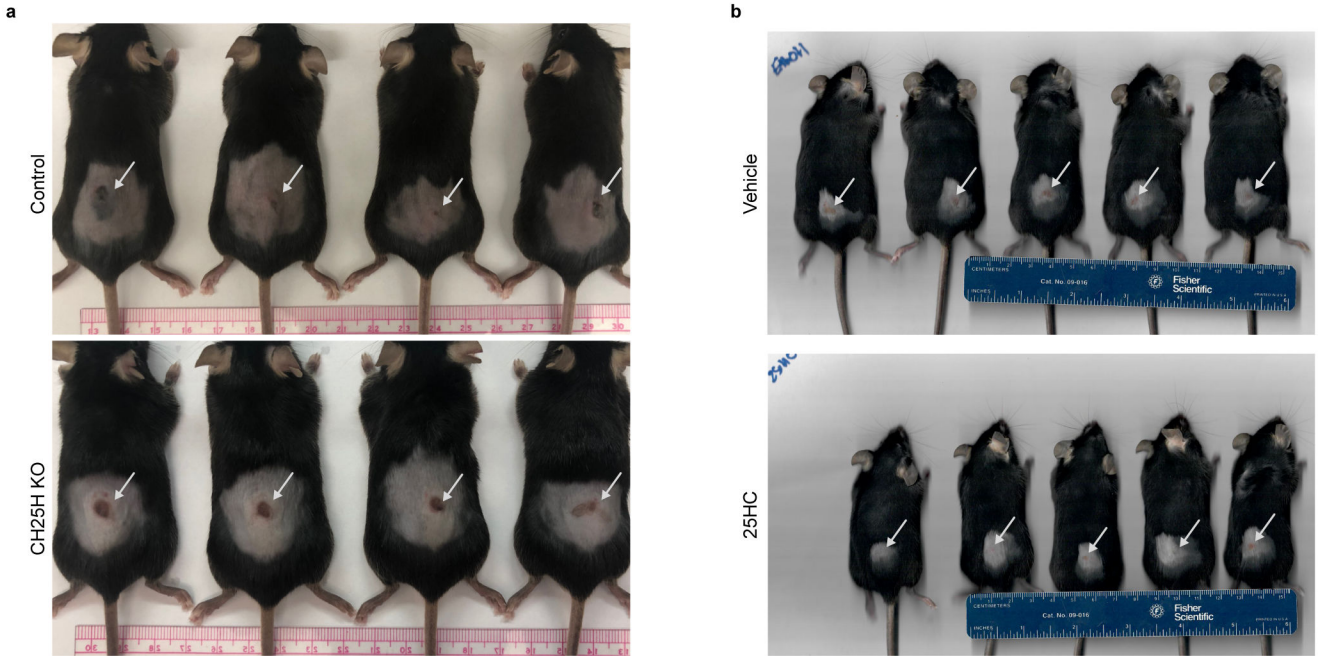

Extended Data Fig. 7.

25HC mediates protection to CDC induced tissue damage. a, Lesion images of control or CH25H KO mice challenged intradermally with SLO (8 kU/mouse) for 48 h. b, Lesion images of vehicle or 25HC pretreated mice challenged intradermally with ALO (20 nM) for 48 h.

Supplementary Material

Refer to Web version on PubMed Central for supplementary material.

Acknowledgements

S.J.B. is supported by NIH AI093768. S.J.B and P.T. are supported by HL146358. E.J.T. was supported by NIH HL136543. M.S.L. is supported by a Ruth L. Kirschstein National Research Service Award AI007323. The research described was also supported by NIH/National Center for Advancing Translational Science (NCATS) UCLA CTSI Grant Number UL1TR001881. We thank S. Young, T. Weston, R.S. Jung for help with protein purification. We thank T. Weston for NanoSIM sample preparation and SEM. We thank A. Divakaruni for guidance with PFO permeabilization assay. We thank A. Radhakrishnan for full-length ALO plasmids. We thank S. Young, A. Hoffmann, Y. Du, R. Sun, T.-T. Wu, J.F. Miller and M. Li for thoughtful discussions.

Data Availability

All original data are available from the corresponding author upon request.

References

1. Lange Y, Swaisgood MH, Ramos BV & Steck TL Plasma membranes contain half the phospholipid and 90% of the cholesterol and sphingomyelin in cultured human fibroblasts. J Biol Chem 264, 3786–3793 (1989). [PubMed: 2917977]
2. Ikonen E Cellular cholesterol trafficking and compartmentalization. Nature reviews. Molecular cell biology 9, 125–138 (2008). [PubMed: 18216769]
3. Van Meer G, Voelker DR & Feigenson GW Membrane lipids: Where they are and how they behave. Nature Reviews Molecular Cell Biology 9, 112–124 (2008). [PubMed: 18216768]
4. Luo J, Yang H & Song BL Mechanisms and regulation of cholesterol homeostasis. Nat Rev Mol Cell Biol 21, 225–245 (2020). [PubMed: 31848472]
5. Blanc M et al. The Transcription Factor STAT-1 Couples Macrophage Synthesis of 25-Hydroxycholesterol to the Interferon Antiviral Response. Immunity 38, 106–118 (2013). [PubMed: 23273843]
6. Reboldi A et al. 25-Hydroxycholesterol suppresses interleukin-1–driven inflammation downstream of type I interferon. Science 345, 679–684 (2014). [PubMed: 25104388]
7. Dang EV, McDonald JG, Russell DW & Cyster JG Oxysterol Restraint of Cholesterol Synthesis Prevents AIM2 Inflammasome Activation. Cell 171, 1057–1071 e1011 (2017). [PubMed: 29033131]
8. Araldi E et al. Lanosterol Modulates TLR4-Mediated Innate Immune Responses in Macrophages. Cell Reports 19, 2743–2755 (2017). [PubMed: 28658622]
9. Blanc M et al. Host defense against viral infection involves interferon mediated down-regulation of sterol biosynthesis. PLoS Biol 9, e1000598 (2011). [PubMed: 21408089]
10. York AG et al. Limiting Cholesterol Biosynthetic Flux Spontaneously Engages Type I IFN Signaling. Cell 163, 1–14 (2015).
11. Shibata N & Glass CK Regulation of macrophage function in inflammation and atherosclerosis. J Lipid Res 50 Suppl, S277–281 (2009). [PubMed: 18987388]
12. Tall AR & Yvan-Charvet L Cholesterol, inflammation and innate immunity. Nat Rev Immunol 15, 104–116 (2015). [PubMed: 25614320]
13. Bauman DR et al. 25-Hydroxycholesterol secreted by macrophages in response to Toll-like receptor activation suppresses immunoglobulin A production. Proc. Natl. Acad. Sci. U.S.A 106, 16764–16769 (2009). [PubMed: 19805370]
14. Liu S-Y et al. Interferon-Inducible Cholesterol-25-Hydroxylase Broadly Inhibits Viral Entry by Production of 25-Hydroxycholesterol. Immunity 38, 92–105 (2013). [PubMed: 23273844]
15. Viard M et al. Role of Cholesterol in Human Immunodeficiency Virus Type 1 Envelope Protein-Mediated Fusion with Host Cells. Journal of Virology 76, 11584–11595 (2002). [PubMed: 12388719]
16. Goluszko P & Nowicki B Membrane Cholesterol: a Crucial Molecule Affecting Interactions of Microbial Pathogens with Mammalian Cells. Infection and Immunity 73, 7791–7796 (2005). [PubMed: 16299268]

17. Rawat SS et al. Modulation of entry of enveloped viruses by cholesterol and sphingolipids. Molecular Membrane Biology 20, 243–254 (2003). [PubMed: 12893532]
18. Mazzon M & Mercer J Lipid interactions during virus entry and infection. Cellular Microbiology 16, 1493–1502 (2014). [PubMed: 25131438]
19. Tweten RK Cholesterol-dependent cytolysins, a family of versatile pore-forming toxins. Infection and immunity 73, 6199–6209 (2005). [PubMed: 16177291]
20. Tweten RK, Hotze EM & Wade KR The Unique Molecular Choreography of Giant Pore Formation by the Cholesterol-Dependent Cytolysins of Gram-Positive Bacteria. Annu Rev Microbiol 69, 323–340 (2015). [PubMed: 26488276]
21. Gilbert RJ Inactivation and activity of cholesterol-dependent cytolysins: what structural studies tell us. Structure 13, 1097–1106 (2005). [PubMed: 16084382]
22. Timmer AM et al. Streptolysin O promotes group A Streptococcus immune evasion by accelerated macrophage apoptosis. J Biol Chem 284, 862–871 (2009). [PubMed: 19001420]
23. Bhattacharjee P & Keyel PA Cholesterol-dependent cytolysins impair pro-inflammatory macrophage responses. Scientific Reports 8, 6458 (2018). [PubMed: 29691463]
24. Corrotte M, Fernandes MC, Tam C & Andrews NW Toxin pores endocytosed during plasma membrane repair traffic into the lumen of MVBs for degradation. Traffic 13, 483–494 (2012). [PubMed: 22212686]
25. McNeil PL & Kirchhausen T An emergency response team for membrane repair. Nat Rev Mol Cell Biol 6, 499–505 (2005). [PubMed: 15928713]
26. Romero M et al. Intrinsic repair protects cells from pore-forming toxins by microvesicle shedding. Cell Death Differ 24, 798–808 (2017). [PubMed: 28186501]
27. Oishi Y et al. SREBP1 Contributes to Resolution of Pro-inflammatory TLR4 Signaling by Reprogramming Fatty Acid Metabolism. Cell Metab 25, 412–427 (2017). [PubMed: 28041958]
28. Stetson DB & Medzhitov R Type I Interferons in Host Defense. Immunity 25, 373–381 (2006). [PubMed: 16979569]
29. McNab F, Mayer-Barber K, Sher A, Wack A & O'Garra A Type I interferons in infectious disease. Nature Reviews Immunology 15, 87–103 (2015).
30. Takeuchi O & Akira S Pattern recognition receptors and inflammation. Cell 140, 805–820 (2010). [PubMed: 20303872]
31. Woodward JJ, Iavarone AT & Portnoy DA c-di-AMP secreted by intracellular Listeria monocytogenes activates a host type I interferon response. Science 328, 1703–1705 (2010). [PubMed: 20508090]
32. Pandey AK et al. NOD2, RIP2 and IRF5 play a critical role in the type I interferon response to Mycobacterium tuberculosis. PLoS Pathog 5, e1000500 (2009). [PubMed: 19578435]
33. Gay A, Rye D & Radhakrishnan A Switch-like responses of two cholesterol sensors do not require protein oligomerization in membranes. Biophysical Journal 108, 1459–1469 (2015). [PubMed: 25809258]
34. Chakrabarti RS et al. Variability of cholesterol accessibility in human red blood cells measured using a bacterial cholesterol-binding toxin. eLife 6, 1–27 (2017).
35. Infante RE & Radhakrishnan A Continuous transport of a small fraction of plasma membrane cholesterol to endoplasmic reticulum regulates total cellular cholesterol. eLife 6, 1–23 (2017).
36. Endapally S, Infante RE & Radhakrishnan A Monitoring and Modulating Intracellular Cholesterol Trafficking Using ALOD4, a Cholesterol-Binding Protein. Methods Mol Biol 1949, 153–163 (2019). [PubMed: 30790255]
37. Maxfield FR & Wustner D Analysis of cholesterol trafficking with fluorescent probes. Methods Cell Biol 108, 367–393 (2012). [PubMed: 22325611]
38. Endapally S et al. Molecular Discrimination between Two Conformations of Sphingomyelin in Plasma Membranes. Cell 176, 1040–1053.e1017 (2019). [PubMed: 30712872]
39. He C et al. High-resolution imaging and quantification of plasma membrane cholesterol by NanoSIMS. Proceedings of the National Academy of Sciences 114, 2000–2005 (2017).
40. He C et al. Macrophages release plasma membrane-derived particles rich in accessible cholesterol. Proceedings of the National Academy of Sciences 115, E8499–E8508 (2018).

41. Kandutsch AA & Chen HW Regulation of sterol synthesis in cultured cells by oxygenated derivatives of cholesterol. J Cell Physiol 85, 415–424 (1975). [PubMed: 164478]
42. Goldstein JL, DeBose-Boyd RA & Brown MS Protein sensors for membrane sterols. Cell 124, 35–46 (2006). [PubMed: 16413480]
43. Panousis CG & Zuckerman SH Regulation of cholesterol distribution in macrophage-derived foam cells by interferon-gamma. J Lipid Res 41, 75–83 (2000). [PubMed: 10627504]
44. Keyel PA, Tkacheva OA, Larregina AT & Salter RD Coordinate stimulation of macrophages by microparticles and TLR ligands induces foam cell formation. J Immunol 189, 4621–4629 (2012). [PubMed: 23018455]
45. Collins JL et al. Identification of a nonsteroidal liver X receptor agonist through parallel array synthesis of tertiary amines. J Med Chem 45, 1963–1966 (2002). [PubMed: 11985463]
46. Das A, Brown MS, Anderson DD, Goldstein JL & Radhakrishnan A Three pools of plasma membrane cholesterol and their relation to cholesterol homeostasis. eLife 3 (2014).
47. Pike LJ Lipid rafts: bringing order to chaos. J Lipid Res 44, 655–667 (2003). [PubMed: 12562849]
48. Das DK, Baker MG & Venugopal K Risk factors, microbiological findings and outcomes of necrotizing fasciitis in New Zealand: a retrospective chart review. BMC Infectious Diseases 12, 348 (2012). [PubMed: 23234429]
49. Arif N, Yousfi S & Vinnard C Deaths from necrotizing fasciitis in the United States, 2003–2013. Epidemiol Infect 144, 1338–1344 (2016). [PubMed: 26548496]

Methods-only References

50. Timmins JM et al. Targeted inactivation of hepatic Abca1 causes profound hypoalphalipoproteinemia and kidney hypercatabolism of apoA-I. J Clin Invest 115, 1333–1342 (2005). [PubMed: 15841208]
51. Sag D, Cekic C, Wu R, Linden J & Hedrick CC The cholesterol transporter ABCG1 links cholesterol homeostasis and tumour immunity. Nat Commun 6, 6354 (2015). [PubMed: 25724068]
52. Divakaruni AS et al. Thiazolidinediones are acute, specific inhibitors of the mitochondrial pyruvate carrier. Proc. Natl. Acad. Sci. U.S.A 110, 5422–5427 (2013). [PubMed: 23513224]
53. Bligh EG & Dyer WJ A rapid method of total lipid extraction and purification. Can J Biochem Physiol 37, 911–917 (1959). [PubMed: 13671378]
54. Williams KJ et al. An essential requirement for the SCAP/SREBP signaling axis to protect cancer cells from lipotoxicity. Cancer Res. 73, 2850–2862 (2013). [PubMed: 23440422]
55. Argus JP et al. Development and Application of FASA, a Model for Quantifying Fatty Acid Metabolism Using Stable Isotope Labeling. Cell Reports 25, 2919–2934.e2918 (2018). [PubMed: 30517876]
56. He C, Fong LG, Young SG & Jiang H NanoSIMS imaging: an approach for visualizing and quantifying lipids in cells and tissues. J. Investig. Med 65, 669–672 (2017).

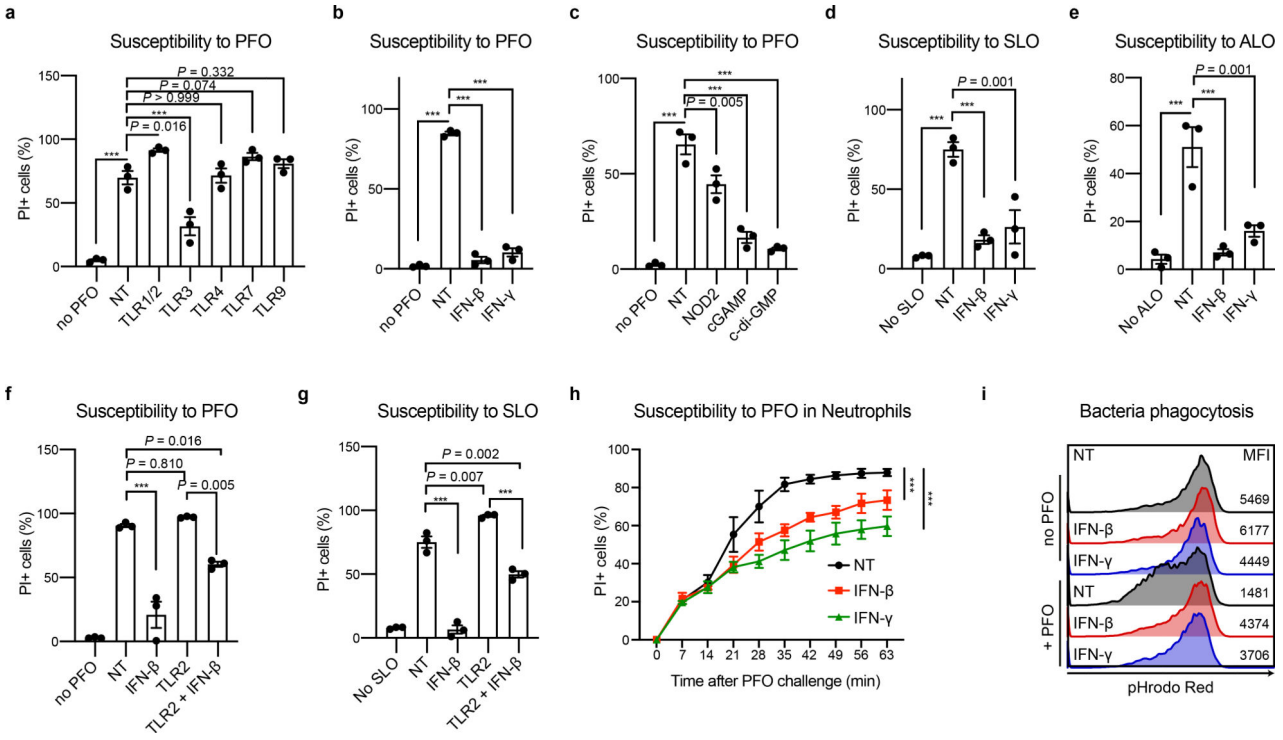

Fig. 1 |. Interferon signaling mediates resistance to cholesterol-dependent cytolysins

a. Percentage of propidium iodide (PI)–positive BMDMs treated with the TLR1/2 agonist (Pam3CSK4; 50 ng/mL), TLR3 agonist (Poly(I:C); 1 μg/mL), TLR4 agonist (LPS; 50 ng/mL), TLR7 agonist (CL307; 100 nM), TLR9 (ODN1668; 100 nM) agonist, or unstimulated (NT) for 24 h and then challenged with perfringolysin O (PFO) for 60 min in the presence of PI.

b. Percentage of PI–positive BMDMs treated with IFN-β (20 ng/mL) and IFN-γ (20 ng/mL) for 24 h and then challenged with PFO for 60 min in the presence of PI.

c. Percentage of PI–positive BMDMs treated with NOD2 agonist (N-Glycolyl-MDP; 20 μg/ml), STING agonist (2',3'cGAMP and c-di-GMP; both 2 μg/mL) for 24 h and then challenged with PFO for 60 min in the presence of PI.

d. Percentage of PI–positive BMDMs treated with the indicated IFNs (20 ng/mL) for 24 h and then challenged with Streptolysin-O (SLO) for 2 h in the presence of PI.

e. Percentage of PI–positive BMDMs treated with the indicated IFNs (20 ng/mL) for 24 h and then challenged with anthrolysin-O (ALO) for 2 h in the presence of PI.

f. Percentage of PI–positive BMDMs treated with TLR1/2 (50 ng/mL) together with IFNs (100 ng/mL) for 24 h and then challenged with PFO for 60 min in the presence of PI.

g. Percentage of PI–positive BMDMs treated with TLR1/2 (50 ng/mL) together with IFNs (100 ng/mL) for 24 h and then challenged with SLO for 2 h in the presence of PI.

h. Percentage of PI–positive neutrophils treated with IFN-β (20 ng/mL) and IFN-γ (20 ng/mL) for 4 h and then challenged with PFO for 60 min in the presence of PI (n = 3).

i. Flow cytometry plots of *S. aureus* phagocytosed by control or IFNs-stimulated BMDMs. Macrophage cultures were stimulated with IFNs (100 ng/mL) for 24 h. BMDMs were then washed and then incubated with PFO for 15 min. PFO containing media was then replaced

with fresh media containing pHrodo-red-labeled *S. aureus*. Median fluorescence intensity (MFI) are indicated on the right.

Data are representatives of three independent experiments. Data in **a**-**h** are shown as mean ± s.e.m.(n=3). Statistical significance was determined using a one-way ANOVA with Dunnett's correction (**a**-**e**), a two-way ANOVA with Tukey's correction (**f, g**), or an RM one-way ANOVA with Dunnett's correction (**h**). ***P<0.001.

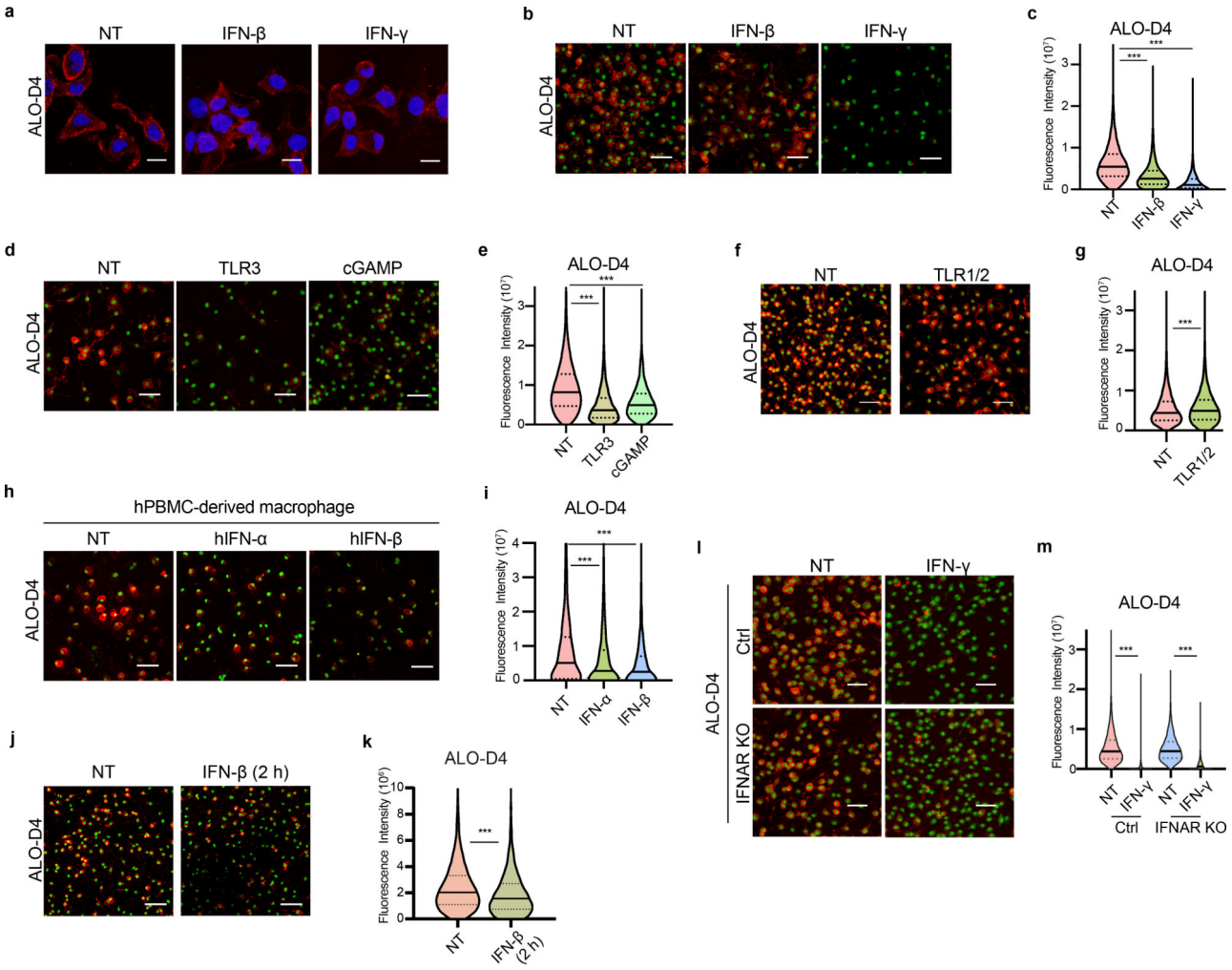

Fig. 2 |. IFN signals decrease plasma membrane binding to ALO-D4 protein

a. Super resolution confocal images of macrophage cultures stimulated with the indicated IFNs (20 ng/mL) for 24 h and then stained with fluorescent ALO-D4 and DAPI.

b. Confocal images of macrophage cultures stimulated with the indicated IFNs (20 ng/mL) for 24 h and then stained with fluorescent ALO-D4 and DAPI.

c. Violin plots of cellular fluorescent intensity quantified from **b** (from left to right: n = 6539, 4561, 5367).

d. Confocal images of macrophage cultures stimulated with the indicated PRR ligands for 24 h and then stained with fluorescent ALO-D4 and DAPI.

e. Violin plots of cellular fluorescent intensity quantified from **d** (n = 5931, 4766, 5660).

f. Confocal images of macrophage cultures stimulated with the indicated TLR agonists for 24 h and then stained with fluorescent ALO-D4 and DAPI.

g. Violin plots of cellular fluorescent intensity quantified from **f** (n = 4358, 3270).

h. Confocal images of human peripheral blood monocyte (hPBMC)–derived macrophages stimulated with human IFN-α or IFN-β (10 ng/mL) for 24 h and then stained with fluorescent ALO-D4 and DAPI.

i. Violin plots of cellular fluorescent intensity quantified from **h** (n = 2084, 1818, 1728).

j. Confocal images of macrophage cultures stimulated with IFN-β (20 ng/mL) for 2 h and then stained with fluorescent ALO-D4 and DAPI.

k. Violin plots of cellular fluorescent intensity quantified from **j** (n = 6550, 7012).

l. Confocal images of WT or type I interferon receptor–deficient (IFNAR KO) BMDMs stimulated with IFN-γ (20 ng/mL) for 24 h and then stained with fluorescent ALO-D4 and DAPI.

m. Violin plots of cellular fluorescent intensity quantified from **l** (n = 4358, 2853, 7089, 5458).

Data in **a** are representatives of three independent samples. Data in **b**-**m** are representatives of three (**b**-**k**) or two (**l**, **m**) independent experiments. Violin plots in **c**, **e**, **g**, **i**, **k**, and **m** are shown with median (solid line) and 25% and 75% percentiles (dashed lines), and statistical significance was determined using a Kruskal-Wallis test with Dunn's correction (**c, e, i**) or a two-tailed Mann-Whitney test (**g**, **k**, **m**). ***P<0.001. Scale bars represent 10 μm (**a**) or 50 μm (**b**, **d**, **f**, **h**, **j, l**).

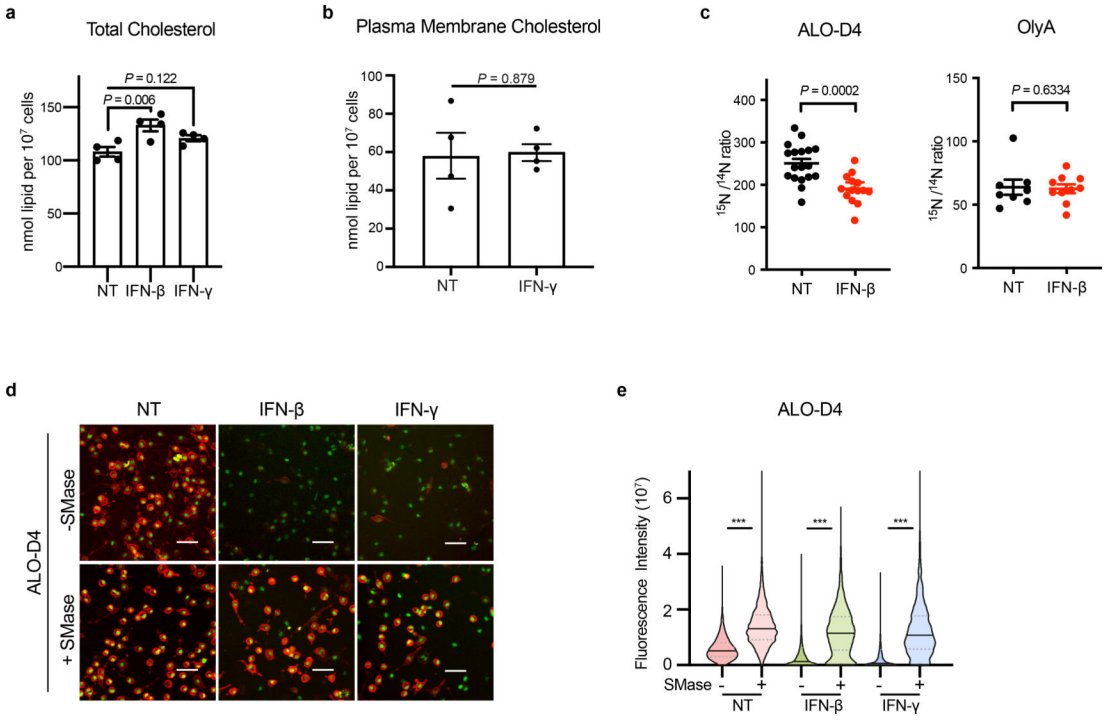

Fig. 3 |. IFN signals reprogram cholesterol metabolism to decrease the pool of cholesterol targeted by CDCs

a. Total cholesterol (nmol/10^7 cells) from C57BL/6 bone marrow–derived macrophages (BMDMs) stimulated with IFN-β (20 ng/mL), IFN-γ (20 ng/mL), or unstimulated (NT) for 48 h. Synthesized cholesterol was determined by GC-MS and isotopomer spectral analysis modeling (n = 4).

b. Total plasma membrane cholesterol (nmol/10^7 cells) from C57BL/6 bone marrow–derived macrophages (BMDMs) stimulated with IFN-γ (40 ng/mL) or unstimulated (NT) for 24 h (n = 4).

c. Quantification of [^{15}N]ALO-D4 or [^{15}N]OlyA binding on untreated or IFN-β (100 ng/mL, 16 h)-stimulated BMDMs determined by NanoSIMS. Quantification based on average ^{15}N/^{14}N ratio by cell. Data are mean ± s.e.m (n = 18, 14 for ALO and n = 8, 10 for OlyA).

d. Confocal images of WT BMDM cultures stimulated with IFNs (20 ng/mL) for 24 h, treated with Sphingomyelinase (SMase; 200 mU/mL) for 30 min at 37 ˚C, and then stained with fluorescent ALO-D4 and DAPI. Scale bars represent 50 μm.

e. Violin plots of cellular fluorescent intensity quantified from **d** (n = 6868, 6811, 3404, 3838, 2930, 2642).

Data are representative of three (**a**, **d**, **e**) independent experiments, three independent samples (**c**) or from 4 biological replicates (**b**). Data in **a**-**c** are shown as mean ± s.e.m., violin plot in **e** is shown with median (solid lines) and 25% and 75% percentiles (dashed lines). Statistical significance was determined using a one-way ANOVA with Dunn's correction (**a**), an unpaired two-tailed Student's *t* test (**b**), or a two-tailed Mann-Whitney test (**c**,**e**). ***P<0.001.

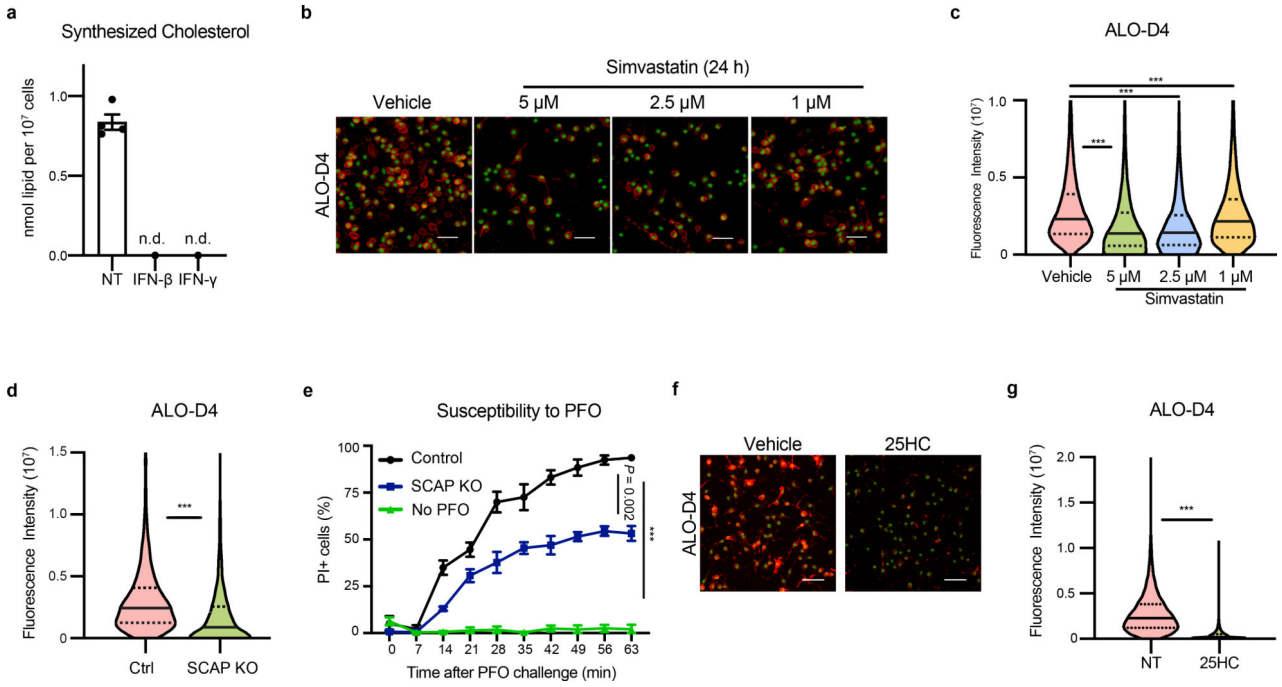

Fig. 4 |. Cholesterol synthesis is linked to CDC susceptibility

a. Net synthesized cholesterol (nmol/10^7 cells) from C57BL/6 bone marrow–derived macrophages (BMDMs) stimulated with IFN-β (20 ng/mL), IFN-γ (20 ng/mL), or unstimulated (NT) for 48 h. Synthesized cholesterol was determined by GC-MS and isotopomer spectral analysis modeling (n = 4).

b. Confocal images of WT BMDM treated with Simvastatin (1 μM-5 μM) for 24 h and then stained with fluorescent ALO-D4 and DAPI.

c. Violin plots of cellular fluorescent intensity quantified from **b** (n = 5713, 2252, 2808, 5556).

d. Violin plots of cellular fluorescent intensity quantified from control or SCAP KO BMDMs stained with fluorescent ALO-D4 and DAPI (n = 3306, 2927).

e. Percentage of PI–positive control or SCAP KO BMDMs challenged with PFO for 60 min in the presence of PI (n = 3).

f. Confocal images of WT BMDMs cultures incubated with 25HC (3 μM) for 4 h, and then stained with fluorescent ALO-D4 and DAPI.

g. Violin plots of cellular fluorescent intensity quantified from **f** (n = 5861, 5769).

Data are representatives of three independent experiments. Data in **a**, and **e** are shown as mean ± s.e.m. Violin plots in **c**, **d,** and **g** are shown with median (solid lines) and 25% and 75% percentiles (dashed lines). Statistical significance was determined using a Kruskal-Wallis test with Dunn's correction (**c**), a two-tailed Mann-Whitney test (**d, g**), or an RM one-way ANOVA (**e**). ***P<0.001. Scale bars in **b** and **f** represent 50 μm.

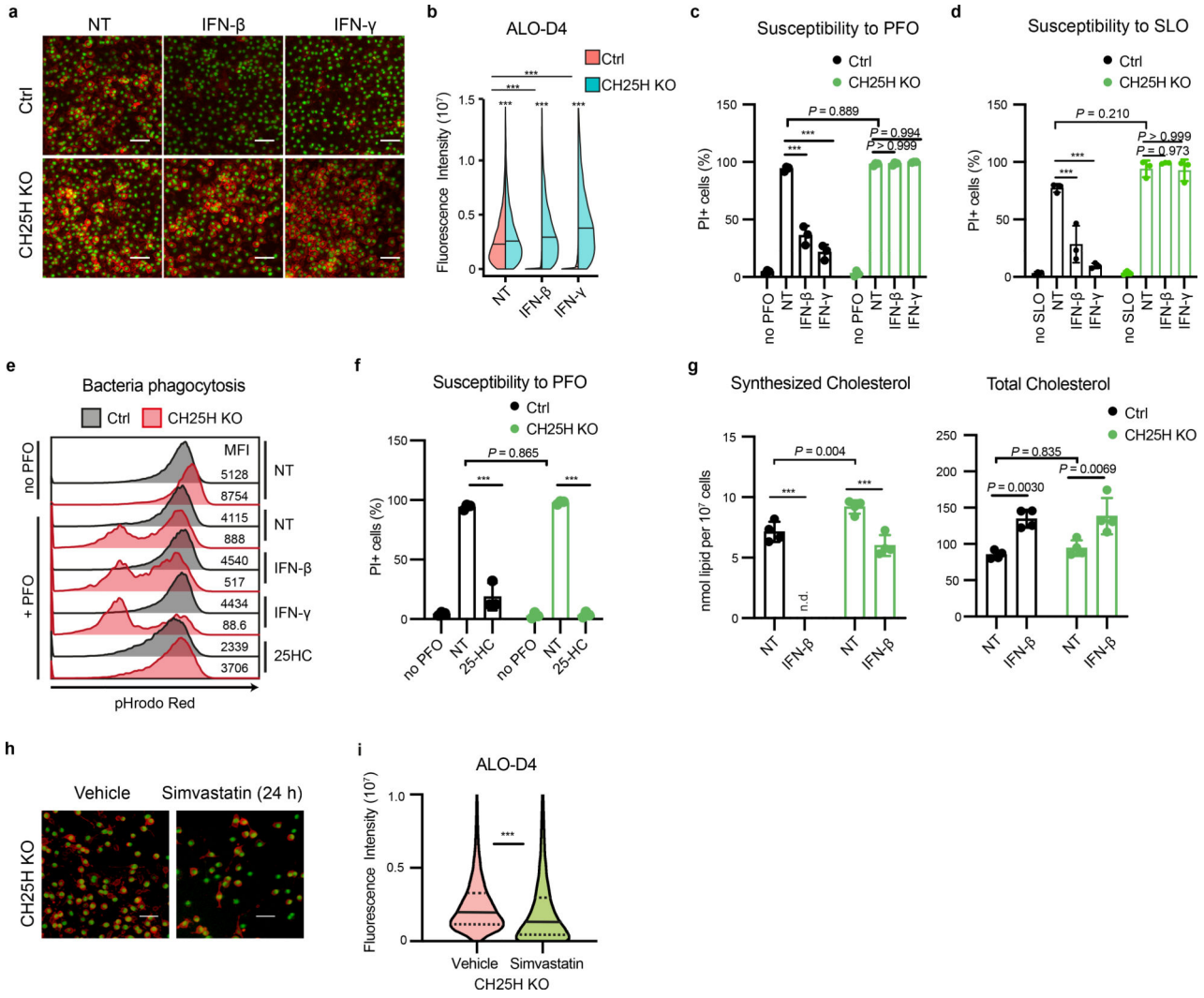

Fig. 5 |. Production of 25-hydroxycholesterol is required to maintain changes in plasma membrane cholesterol and mediates resistance to CDCs

a. Confocal images of control or cholesterol 25-hydroxylase-deficient (CH25H KO) BMDMs cultures stimulated with IFN-β (20 ng/mL), or IFN-γ (20 ng/mL) for 24 h, and then stained with fluorescent ALO-D4 and DAPI.

b. Violin plots of cellular fluorescent intensity quantified from **a** (from left to right: n = 5294, 5505, 4564, 4066, 5370, 4962).

c. Percentage of PI-positive control or CH25H KO BMDMs stimulated with IFNs (20 ng/mL) for 24 h and then challenged with PFO for 60 minutes in the presence of PI.

d. Percentage of PI-positive control or CH25H KO BMDMs stimulated with IFNs (20 ng/mL) for 24 h and then challenged with SLO for 2 h in the presence of PI.

e. Flow cytometry plots of *S. aureus* phagocytosed by control or CH25H KO BMDMs. Macrophage cultures were treated with IFNs (100 ng/mL) or 25HC (3 μM). After 24 h, BMDMs were washed and then incubated with PFO for 15 min. PFO containing media was then replaced with fresh media containing pHrodo-red-labeled *S. aureus*. Median fluorescence intensity (MFI) are indicated on the right.

f. Percentage of PI-positive control or CH25H KO BMDMs incubated with 25HC (1 μM) overnight and then challenged with PFO for 60 minutes in the presence of PI.
g. Net synthesized and total cholesterol (nmol/10^7 cells) from CH25H-deficient or control bone marrow–derived macrophages (BMDMs) stimulated with IFN-β (20 ng/mL) or unstimulated (NT) for 48 h. Synthesized cholesterol was determined by GC-MS and isotopomer spectral analysis modeling.
h. Confocal images of CH25H KO BMDMs treated with Simvastatin (5 μM) for 24 h and then stained with fluorescent ALO-D4 and DAPI.
i. Violin plots of cellular fluorescent intensity quantified from **h** (n = 6666, 2867).
Data are representative of three independent experiments. Data in **c**, **d**, **f**, and **g** are shown as mean ± s.e.m. (n = 3 in **c**, **d**, **f** and n = 4 in **g**). Violin plots are show with median (solid lines in **b**, **i**) and 25% and 75% percentiles (dashed lines in **i**). Statistical significance was determined using a Kruskal-Wallis test with Dunn's correction (**b**), a two-way ANOVA with Tukey's correction (**c**, **d**, **f**, **g**), or a two-tailed Mann-Whitney test (**i**). ***P<0.001. Scale bars in **a** and **h** represent 50 μm.

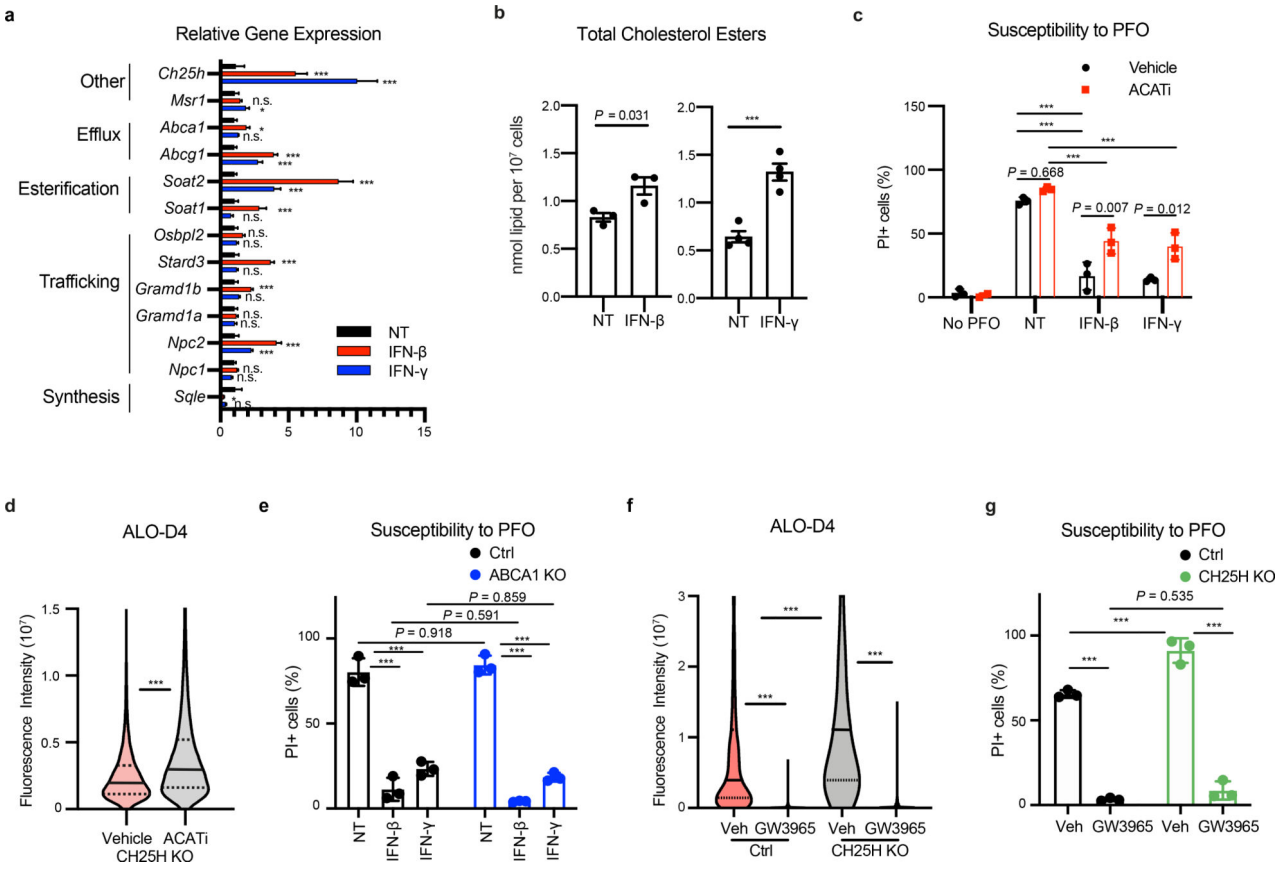

Fig. 6 |. Cholesterol esterification contributes to CDC resistance of macrophages

a. qPCR analysis of genes that regulate cholesterol homeostasis in WT BMDM treated with IFNs (20 ng/mL) for 24 h.

b. Quantification (nmol/10^7 cells) of total cholesterol ester (CE) in WT BMDMs stimulated with IFN-β (20 ng/mL) or IFN-γ (20 ng/mL) for 48 h. CE pool sizes were determined by direct infusion mass spectrometry (left panel: n = 3, right panel: n = 4).

c. Percentage of PI–positive BMDMs treated with IFN-β (20 ng/mL) and IFN-γ (20 ng/mL) for 24 h in the presence of the ACAT inhibitor 58–035 (4.3 μM) and then challenged with PFO for 60 min in the presence of PI.

d. Violin plots of cellular fluorescent intensity quantified from control or CH25H KO BMDMs treated with ACAT inhibitor 58–035 (4.3 μM) for 24 h and then stained with fluorescent ALO-D4 and DAPI (n = 6666, 9997).

e. Percentage of PI–positive control or ABCA1 KO BMDMs stimulated with IFNs (20 ng/mL) for 24 h and then challenged with PFO for 60 minutes in the presence of PI.

f. Violin plots of cellular fluorescent intensity quantified from control or CH25H KO BMDMs treated with LXR agonist GW3965 (1 μM) for 24 h and then stained with fluorescent ALO-D4 and DAPI (n= 2304, 3954, 2712, 2322).

g. Percentage of PI–positive control or CH25H KO BMDMs treated with LXR agonist GW3965 (1 μM) for 24 h and then challenged with PFO for 60 min in the presence of PI.

Data are representative of three independent experiments. Data in **a, b, c, e,** and **g** are shown as mean ± s.e.m. (n = 3) unless otherwise specified. Violin plots in **d**, and **f** are shown with

median (solid lines) and 25% and 75% percentiles (dashed lines). Statistical significance was determined using a one-way ANOVA with Dunnett's correction (**a**), an unpaired two-tailed Student's *t* test (**b**), a two-way ANOVA with Tukey's correction (**c**, **e**, **g**), a two-tailed Mann-Whitney test (**d**), or a Kruskal-Wallis test with Dunn's correction (**f**). ***$P<0.001$, n.s., not significant.

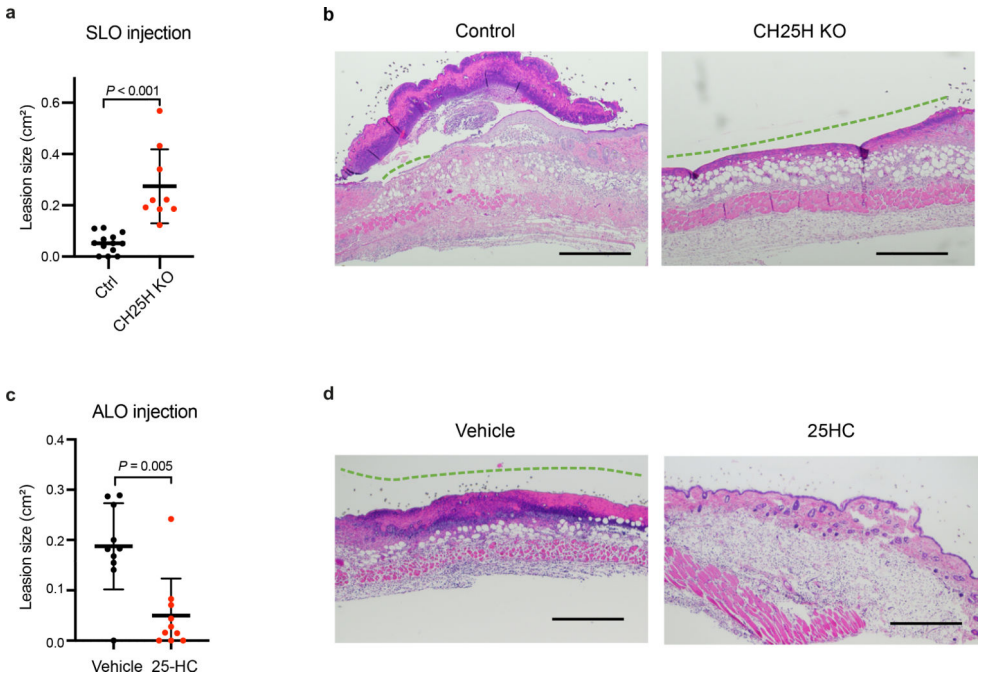

Fig. 7 |. 25HC mediates protection to CDC induced tissue damage

a. Quantification of lesion size from WT (n = 13) and CH25H KO mice (n = 9) challenged with SLO for 48 h.

b. Representative histology from mice demonstrates serum crust overlying partial thickness erosion with a small full-thickness ulceration (green dotted line) of the epidermis, and a robust inflammatory response in the dermis and adipose tissue in control (B6) mice (left panel). Wound areas in CH25H-deficient mice demonstrate a large ulceration (green dotted line) with necrosis/destruction of the papillary and much of the reticular dermis with a less pronounced inflammatory response (right panel).

c. Quantification of lesion size from WT mice (n = 10 each) pre-treated with vehicle or 25HC for 6 h and challenged with ALO for 48 h.

d. Representative histology of wounds demonstrates full thickness ulceration (green dotted line) with overlying neutrophilic/serum crust by ALO in wounds pretreated with ethanol vehicle (left panel), but no ulceration and only edema and a mixed mononuclear and neutrophilic inflammatory host response in the dermis and adipose tissue of mice pretreated with 25HC (right panel).

Data in **a**, **c** are shown as mean ± s.e.m. and statistical significance was determined using a two-tailed Mann-Whitney test. Scale bars in **b**, **d** represent 500 μm.